

AD _____

GRANT NUMBER DAMD17-94-J-4359

TITLE: Amplified Genes in Breast Cancer: Molecular Targets for Investigation and Therapy

PRINCIPAL INVESTIGATOR: Geoffrey M. Wahl, Ph.D.

CONTRACTING ORGANIZATION: Salk Institute for Biological Studies
La Jolla, California 92037-1099

REPORT DATE: September 1998

TYPE OF REPORT: Annual

PREPARED FOR: Commander
U.S. Army Medical Research and Materiel Command
Fort Detrick, Frederick, Maryland 21702-5012

DISTRIBUTION STATEMENT: Approved for public release;
distribution unlimited

The views, opinions and/or findings contained in this report are those of the author(s) and should not be construed as an official Department of the Army position, policy or decision unless so designated by other documentation.

REPORT DOCUMENTATION PAGE

Form Approved

OMB No. 0704-0188

Public reporting burden for this collection of information is estimated to average 1 hour per response, including the time for reviewing instructions, searching existing data sources, gathering and maintaining the data needed, and completing and reviewing the collection of information. Send comments regarding this burden estimate or any other aspect of this collection of information, including suggestions for reducing this burden, to Washington Headquarters Services, Directorate for Information Operations and Reports, 1215 Jefferson Davis Highway, Suite 1204, Arlington, VA 22202-4302, and to the Office of Management and Budget, Paperwork Reduction Project (0704-0188), Washington, DC 20503.

1. AGENCY USE ONLY (Leave blank)		2. REPORT DATE September 1998	3. REPORT TYPE AND DATES COVERED Annual (1 Sep 97 - 31 Aug 98)	
4. TITLE AND SUBTITLE Amplified Genes in Breast Cancer: Molecular Targets for Investigation and Therapy			5. FUNDING NUMBERS DAMD17-94-J-4359	
6. AUTHOR(S) Geoffrey M. Wahl, Ph.D.				
7. PERFORMING ORGANIZATION NAME(S) AND ADDRESS(ES) Salk Institute for Biological Studies La Jolla, California 92037-1099			8. PERFORMING ORGANIZATION REPORT NUMBER	
9. SPONSORING/MONITORING AGENCY NAME(S) AND ADDRESS(ES) Commander U.S. Army Medical Research and Materiel Command Fort Detrick, Frederick, MD 21702-5012			10. SPONSORING/MONITORING AGENCY REPORT NUMBER	
11. SUPPLEMENTARY NOTES			19990820 016	
12a. DISTRIBUTION / AVAILABILITY STATEMENT Approved for public release; distribution unlimited			12b. DISTRIBUTION CODE	
13. ABSTRACT (Maximum 200) We showed earlier that micronucleation reduces the number of double minute chromosomes (DMs) containing amplified oncogenes and correlates with reduced tumorigenicity. We investigated the mechanism of micronucleation using a novel fluorescent chromosome labeling system we developed to study the distribution of DMs in living cancer cells. Our results demonstrate that DMs often cluster and form bridges between segregating daughter chromosomes during anaphase. Time-lapse observations revealed that cytokinesis severed DM bridges, and resulted in their uneven distribution to daughter cells. Occasionally, clustered DMs lagged behind pole-ward moving chromosomes and formed separate micronuclei. To further analyze DM behavior, we specifically labeled DMs using a lactose-operator/lactose-repressor-GFP system. We found that DMs appeared randomly dispersed in interphase nuclei, but later in prophase, they attached to the periphery of condensed prophase chromosomes. DMs appear to move to the nuclear periphery during chromosome condensation, make clusters, and continue to associate with chromosome arms throughout cytokinesis. Occasionally, this association is disrupted and results in micronucleation. The DM specific labeling system will not only be useful for detailed analyses of DM dynamics but will also greatly facilitate the screening of drugs which efficiently eliminate DMs from cancer cells.				
14. SUBJECT TERMS Gene Amplification, Cytogenetics, Double Minutes, Treatment, Oncogenes, New Biomarkers, Humans, Clinical Trials, Anatomical Samples, Breast Cancer			15. NUMBER OF PAGES 36	
			16. PRICE CODE	
17. SECURITY CLASSIFICATION OF REPORT Unclassified	18. SECURITY CLASSIFICATION OF THIS PAGE Unclassified	19. SECURITY CLASSIFICATION OF ABSTRACT Unclassified	20. LIMITATION OF ABSTRACT Unlimited	

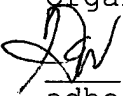
FOREWORD

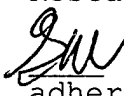
Opinions, interpretations, conclusions and recommendations are those of the author and are not necessarily endorsed by the U.S. Army.

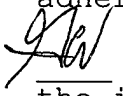
____ Where copyrighted material is quoted, permission has been obtained to use such material.

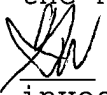
____ Where material from documents designated for limited distribution is quoted, permission has been obtained to use the material.

____ Citations of commercial organizations and trade names in this report do not constitute an official Department of Army endorsement or approval of the products or services of these organizations.

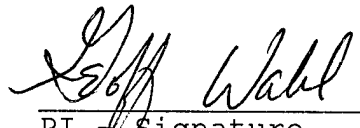
 In conducting research using animals, the investigator(s) adhered to the "Guide for the Care and Use of Laboratory Animals," prepared by the Committee on Care and Use of Laboratory Animals of the Institute of Laboratory Resources, National Research Council (NIH Publication No. 86-23, Revised 1985).

 For the protection of human subjects, the investigator(s) adhered to policies of applicable Federal Law 45 CFR 46.

 In conducting research utilizing recombinant DNA technology, the investigator(s) adhered to current guidelines promulgated by the National Institutes of Health.

 In the conduct of research utilizing recombinant DNA, the investigator(s) adhered to the NIH Guidelines for Research Involving Recombinant DNA Molecules.

____ In the conduct of research involving hazardous organisms, the investigator(s) adhered to the CDC-NIH Guide for Biosafety in Microbiological and Biomedical Laboratories.


PI Signature

9-15-98
Date

TABLE OF CONTENTS

	Page
Front Cover	1
SF298 Report Documentation Page	2
Foreword	3
Table of Contents	4
Introduction	5
Body (Methods and Results)	6
Conclusion	8
References	10
Appendices	
A. Figures	10
B. Bibliography	11
C. Personnel Supported	11

Introduction

Loss of genetic stability occurs frequently during the development of human cancers, and can manifest itself as gene amplification (1, 2). Genes can be amplified within acentric, autonomously replicating extrachromosomal molecules referred to as double minute chromosomes (DMs), or within expanded chromosomal regions (i.e., HSRs) (3, 4). It has been reported that DM-mediated gene amplification is more predominant than HSRs in tumor biopsies (5).

Our previous studies showed that genes amplified in DMs can be selectively entrapped in micronuclei, which we hypothesized mediate their elimination from tumor cells (6-8). We showed that treatment with a variety of agents used at concentrations that interfere with, but do not completely inhibit, DNA replication, can dramatically increase micronucleation frequency and DM loss rate (6-9). The micronuclei appear to be formed by either the well known post-mitotic mechanism or by our proposed novel mechanism involving the budding of the nuclear membrane in S-phase (8). Micronuclei capture acentric fragments 100-1000 times more frequently than they entrap chromosomes (7). Importantly, the drugs that induce micronucleation efficiently in tumor cells do not induce them in normal cells (8). As inactivating p53 in the normal cells enables these agents to induce micronucleation (8), we infer that this effect should be restricted to cells with a defective p53 pathway (10). In view of the selective capture of DMs by the micronucleation process, the effects of this treatment strategy on normal tissue should be minimal.

The gene copy reduction achieved by micronuclear capture of DMs is sufficient to reduce tumorigenicity in several model systems (6, 11). An important implication of this observation is that while the cancer cell has many genetic alterations, gene overexpression resulting from DMs must be rate limiting for growth. The long term goal of this research has been to develop strategies to efficiently eliminate DMs from tumor cells. For this purpose, we needed to investigate the mechanisms of DM elimination with greater sensitivity than that afforded by conventional methods. This is challenging because DMs are far smaller than normal chromosomes, and have not been observed in living (unfixed) cells until recently (12). We therefore developed a new technology to enable the live detection of DMs throughout the cell cycle.

The first generation of this technology was described in the last progress report. This system utilizes a retroviral vector encoding the human histone H2B gene fused to the *Aequorea victoria* green fluorescent protein (H2B-GFP) (12) in which the codons have been optimized for expression in mammalian cells. Chromosomes in cells infected with the H2B-GFP virus are fluorescently labeled, as the H2B-GFP fusion protein is incorporated into their nucleosomes. The H2B-GFP strategy has several advantages over staining with fluorescent dyes including far less toxicity, minimal photobleaching, and long-term tagging of chromosomes through continuous expression (12).

We have made significant progress during the past year with the observation of DMs in living cancer cells. First, we used the H2B-GFP labeling system to examine the localization of DMs and documented their unusual "clustering" behavior during mitosis. Using time-lapse fluorescent microscopy, we observed the segregation of DMs during mitosis and their incorporation into micronuclei in living cancer cells. Finally, we developed a system to specifically and fluorescently tag DMs and observe DM dynamics throughout the cell cycle of live cells. This 'second generation' labeling system will greatly facilitate the screening of drugs which efficiently eliminate DMs from cancer cells, and will enable us to analyze the behavior of DM-containing tumor cells in animals, and the effects of DM-elimination agents identified in our in vitro screen on DM retention and tumor cell viability in vivo.

Methods and Results

I Visualization of DMs in living cancer cells using the H2B-GFP chromosome labeling system

i) Confocal microscopic observation of DMs in living cancer cells

The highly sensitive H2B-GFP chromosome labeling technique was used to detect DMs in living cancer cells (12). A colon cancer of neuroendocrine origin (COLO320DM), which contains numerous DMs encoding the c-myc oncogene (13) was infected with the H2B-GFP retrovirus. Over 90% of the cells expressed H2B-GFP protein by two days after infection. The H2B-GFP expressing cells were seeded in a Dvorak-Stotler chamber (Lucas-Highland Company), a special chamber designed for live observation, and serial sectioned images were collected using confocal microscopy. This enabled the high resolution imaging of chromosomes with minimal effects on cellular structure. In mitotic cells, we frequently observed small fluorescent dots (Fig. 1a, b), and the sizes of these dots (0.7-0.85 microns in diameter) correspond to that of the DMs in this cell line. These fluorescent particles frequently clustered in anaphase cells and attached to chromosomes (Fig 1a). Occasionally, they aligned in regular arrays and formed extended bridges between segregating daughter chromosomes (Fig. 1b). To confirm that these dot-like chromatin bodies were DMs, mitotic COLO320DM cells were fixed without colcemid treatment, and the DM distribution was analyzed by fluorescence in situ hybridization (FISH) using a c-myc cosmid probe. While chromosome spreads of colcemid treated cells usually showed dispersed DMs (Fig. 1c), untreated mitotic cells frequently contained clusters of DMs (Fig. 1d, e). By FISH, the DM distribution patterns were strikingly similar to the dot-like structures observed in H2B-GFP expressing cells (compare Fig. 1a, b, and d, e). The results strongly suggest that the dot like chromatin bodies we observed in living cells represent DMs. We found that most of the observed mitotic cells contained clusters of DMs, though the number of DMs varied among cells. Approximately 30% of the anaphase cells we detected contained 'DM bridges'. Thus, the clustering and unbalanced distribution of DMs to daughter cells during mitosis is common in this cell line. Given the small size of DMs (averaging 2 megabases in this cell line), our data clearly demonstrate the sensitivity of the H2B-GFP detection strategy and further establish the feasibility of this method for analyzing DM behavior over time in cycling cells.

ii) Time-lapse observation of DM segregation and micronucleation reveals their unusual behavior in mitotic cells

We analyzed DM segregation during mitosis by time-lapse observations using an epifluorescence microscope equipped with a video camera (12). As described above, DMs often cluster in anaphase cells and attach to groups of segregating chromosomes. Occasionally, segregating daughter chromosomes were connected by DM bridges spanning the midplane of anaphase cells (Fig. 2A). DM bridges appeared to stretch as daughter chromosomes segregated, and were subsequently severed by cytokinesis. The released DM clusters distributed unevenly to daughter nuclei.

We showed previously that DMs replicate according to the cellular program, and that they contain at least one functional replication origin (14). However, during mitosis, as DMs lack functional centromeres, sister minute chromosomes do not separate and consequently produce paired structures which remain associated during mitosis. Our observations show that the clusters of DMs appear to distribute randomly among daughter cells. Such uneven distribution of DMs during mitosis generates daughter cells with an unequal copy number of DM-encoded oncogenes, which is likely to contribute to survival advantages during tumor progression. These observations confirm and extend the model of DM segregation and unequal distribution to daughter cells (15).

We also observed that clusters of DMs lagged behind as normal chromosomes migrated toward opposing poles during anaphase. These clusters separated from the groups of segregating normal chromosomes and became enclosed within separate micronuclei (Fig. 2B). This observation explains why some micronuclei contain numerous DMs yet no chromosomes (7).

Successful observations of DM behavior and micronucleation in living cancer cells will enable further characterization of the effects of various anti-cancer drugs on DM elimination at the single cell level.

II Differential fluorescent tagging of DMs, chromosomes, and nuclear membranes for detailed analyses of DM behavior in living cancer cells

i) DM-specific labeling using the lac operator/lac repressor-GFP system

The results obtained with the H2B-GFP system shows that the real-time tracking of DMs can provide important clues in identifying the mechanisms of DM elimination. However, this strategy labels all chromatin, and the chromosomes produce far more signal than the DMs. The high background fluorescence of the chromosomes in interphase cells precludes analysis of DM behavior with maximal sensitivity and specificity. We, therefore, developed an additional approach to specifically tag DMs with a fluorescent marker in living cells.

DM labeling was achieved using the lac operator/lac repressor-GFP system described recently by Belmont and colleagues (16). This system enables fluorescent labeling of specific chromosomal regions through interaction of integrated lac operator sequences (lac-O) with a lac-repressor-GFP fusion protein (lac-R-GFP). Previous studies showed that this system enables the analysis of an amplified chromosomal region in a Chinese hamster ovary (CHO) cell line (16).

Our recent work indicated that DMs tend to localize to the nuclear periphery during interphase (8). This raised the question of whether DMs might be preferred targets for integration of transfected DNA. Several types of vectors were electroporated into COLO320DM cells to determine whether any would integrate preferentially into DMs. We found that Epstein Barr Virus (EBV) vectors, capable of autonomous replication (17), frequently target DM, raising the possibility that they could be used to introduce exogenous DNA sequences into DMs. This possibility was tested using an EBV vector containing 256 copies of a lac-O repeat (~10 kb) and a blasticidin gene as a drug-resistance marker (T. Kanda and G.M. Wahl, manuscript in preparation). The vector (approximately 19 kb) was then transfected into COLO320DM and the transfected cells were cultured for 2 weeks with blasticidin. The blasticidin-resistant colonies were expanded and 12 independent cell lines were established. We chose three clones to examine the localization of both integrated lac-O DNA and DMs using lac-O repeat and the c-myc cosmid sequences as probes. Two-color FISH analyses revealed that the lac-O repeat colocalized with DMs in the majority of the examined metaphase spreads (Fig. 3A) and micronuclei (not shown). The colocalization of lac-O with c-myc sequences was confirmed to be due to the integration of lac-O repeat into DMs by analysis of stretched chromatin fibers hybridized with probes derived from the lac-O repeat plasmid and c-myc cosmid (Fig. 3B) (18). We observed arrays of the lac-O signals on the same DNA fibers on which c-myc signals were detected, indicating that the transfected sequences integrated into DM DNA. No colocalization of lac-O with normal chromosomes was observed, suggesting that DMs are the preferred targets for EBV integration.

The targeted integration of the transgene enabled the specific labeling of DMs in live cells by expressing the lac-R-GFP fusion protein which binds the integrated lac-O repeat sequence with high affinity. A retroviral vector expressing the lac-R-GFP fusion protein was constructed, and used to infect the cell lines with lac-O integrated into DMs. Two days after infection, cells were fixed and DNA was counterstained with DAPI. We observed bright fluorescent dots in interphase nuclei (Fig. 4a), fluorescent dots attached to the periphery of condensed prophase chromosomes (Fig. 4b), and dots that appeared to attach to segregating daughter chromosomes in anaphase cells (Fig. 4c). We also observed that fluorescent dots representing DMs were incorporated into micronuclei (data not shown). The cellular distribution of these fluorescent dots corresponds well with the known localization of DMs observed by FISH experiments (12). Taken together, DMs appear to move to the nuclear periphery during chromosome condensation, make clusters, and continue to associate with normal chromosomes until completion of cytokinesis. Occasionally, this association is disrupted and results in micronucleation. The sum of these results clearly demonstrates that lac-O repeats are specifically introduced into DMs, and that such DMs can be detected by expressing the lac-R-GFP fusion protein.

ii) Multicolor labeling using different color versions of GFP

As different color versions of GFP protein, such as cyan (CFP) and yellow (YFP), are now available, we should be able to differentially label DMs and chromosomes. These fluorophores can be distinguished using appropriate excitation wavelengths and emission filters. We further established the feasibility of this multicolor approach in cellular analyses by labeling DMs and entire chromosomes using lac-R-YFP and H2B-CFP, respectively. We prepared retroviral vectors expressing either lac-R-YFP or H2B-CFP. COLO320DM cells containing lac-O repeat sequences within their DMs were infected with the two different viruses simultaneously. Our preliminary data indicate that DM signals (yellow) and chromosomes (cyan) can be detected in the same cell using the special filter sets optimized for detecting YFP and CFP, respectively.

The S-phase DM micronucleation hypothesis implicates the nuclear membrane and the lamins as active participants in the budding process (8). To further test this model, we also made a retroviral construct expressing lamin B receptor-CFP (LBR-CFP) fusion protein, which specifically labels inner nuclear membrane (19) (O. Vafa, G.M. Wahl, unpublished). Simultaneous infection of two different retroviruses, expressing lac-R-YFP and LBR-CFP, will label DMs with YFP and nuclear membranes with CFP. This will enable synchronous observations of DM movement relative to nuclear membranes and clarify the possible role of nuclear membranes during micronucleation process.

The technology developed in our lab will enable us to study the dynamics of DM behavior within the nuclei of living cells, and will further reveal details of the micronucleation process *in vivo*. The precision and flexibility in detection offered by this system is not achievable by any other known method. The system also enables efficient screening of chemotherapeutic drugs which accelerate DM elimination.

Conclusion

In the past year, we focused on using the H2B-GFP strategy to analyze DM movements in living cells, and we established a novel technology to label DMs specifically. Using the H2B-GFP chromosome labeling system, we made several important observations which greatly increased our basic knowledge of DM behavior (12). We reported for the first time, the observation of DMs in living cancer cells and we tracked their behavior by time-lapse studies during mitosis. The results revealed the unusual behavior of DMs during mitosis, including their clustering and their association with segregating normal chromosomes (e.g. DMs "hitch-hiking" on chromosomes). Our observations explain how DMs are maintained in cancer cells in spite of their lack of functional centromeres and validates an existing model that DMs can increase their copy number by uneven distribution among daughter cells (15). This system has also attracted a huge amount of attention in the scientific community, as evidenced by the large numbers of requests we have obtained from researchers investigating all facets of biology.

We further established a novel system to specifically label DMs in living cancer cells. The lac-O/lac-R-GFP strategy offers significant advantages for detecting and analyzing DMs. This system enables rapid and sensitive DM localization in interphase and mitotic cells. Since lac-R-GFP is expressed by retroviral infection of cell lines with integrated lac-O, fluorescent signals representing DMs can be detected immediately after simple fixation. By contrast, DM detection by FISH usually takes two or more days. Also, nuclear and chromosomal structures can be preserved better using the lac-R-GFP system than with FISH, since the latter requires denaturation of chromosomal DNA and is known to cause blurring of fine structures (16). We confirmed this by showing that the lac-O/lac-R-GFP system provided far more distinct images of DMs than obtained with the best FISH analyses. To our knowledge, this is the only system currently available for the specific analysis of DMs in cycling live cells. Moreover, we can now differentially label DMs, chromosomes, and nuclear membranes using different color versions of GFP proteins to closely monitor the micronucleation of DMs.

Initial results obtained using the lac-O/lac-R-GFP system demonstrated that DMs attached to the periphery of condensed prophase chromosomes. The results suggest that DMs move to the nuclear periphery during prophase, make clusters, and continue to be associated with normal

chromosomes until the completion of cytokinesis. Occasionally, this association is disrupted and results in micronucleation. These findings have provided us with direction to identify mechanisms which increase the efficiency of micronucleation and DM elimination. We can now begin to identify drugs which affect the clustering of DMs. It is important to determine whether existing agents have collateral activities that enhance DM clustering and elimination. Also, agents that disrupt the association between DM clusters and normal chromosomes is likely to increase micronucleation frequency. The live observation of DMs will enable us to analyze the effect of candidate drugs on DM elimination at the single cell level, as well as in vivo.

Throughout our experiments, we used a colon cancer cell line (COLO320DM) as a model system to study DM behavior in cancer cells (6-8, 12). Our efforts to identify breast cancer cell lines harboring DMs had been complicated by outgrowth of variants which had lost DMs or in which the DM sequences were integrated into chromosomes (5). We found that MDA-MB361, which was reported to have DMs according to ATCC catalog, actually retained very few DMs and was not suitable for live observation studies. However, we have recently found a breast cancer cell line (SW-527, ATCC CRL-7940) which has numerous DMs in most of the metaphase spreads examined. We will apply the DM labeling strategy described above to a broad spectrum of cancer cell lines harboring DMs, including SW-527. We expect that the results obtained by the series of experiments using COLO320DM cells will be generalized to other cancer cells including breast cancer origin. We have already observed the clustering and hitch-hiking behavior of DMs in another colon cancer cell line (SW-613). Thus, it is likely that the clustering and hitch-hiking behavior is a common feature of DMs in various cancer cells.

We have accomplished almost all of the goals proposed for this year, but the time spent in technological development precluded our analysis of whether the H2B-GFP would enable rapid identification of DMs in human biopsy specimens. However, we confirmed the usefulness of this vector by successful DM labeling in a variety of cancer cells, including a breast cancer cell line (SW-527), colon cancer cell line (SW-613), and neuroblastoma cell line (CRL-2270). As the H2B-GFP system is the only system which enables rapid observation of DMs in living cells, we will pursue the possibility of applying this system for clinical diagnosis, expecting that this strategy will overcome the detection limits of the conventional cytogenetic methods.

The technology we have developed in the last year will greatly facilitate several types of analysis in the future that could have significant impact on our understanding of cancer cell behavior in vivo, and on the development of drugs targeted against genetic abnormalities that are unique to cancer cells. We have developed powerful, sensitive and rapid means of labeling tumor cells with fluorescent tags to enable their detection in vivo. This will enable us to address the long-standing question of whether DMs are found frequently in cancers in vivo because their unequal segregation provides a facile genetic strategy for generating tumor cell heterogeneity. We will also be able to screen rapidly for drugs that eliminate DMs through micronucleation. Our fluorescent tagging methods should facilitate automation of such screens, which will enable analysis of large numbers of candidate drugs. This should in turn provide additional insight into the various factors that contribute to the micronucleation process. Finally, having the fluorescently tagged cells and tumors, and DM eliminating agents in hand, we should be able to develop mouse models of metastatic cancer with which we can study with great sensitivity the effects of these agent on tumorigenicity in vivo. This should avail us of new classes of drugs that are tumor specific due to their ability to target genetic abnormalities and mechanisms that are restricted to tumor cells.

Figure legends

Figure 1

DMs cluster in anaphase cells. (a, b) Confocal microscopic images of live COLO320DM cells expressing H2B-GFP. Clustered dot-like chromatin bodies (shown by arrowheads) together with segregating daughter chromosomes are visualized by GFP fluorescence (green). The scale bars are 5 μ m. (c) DMs were detected in a metaphase spread of colcemid-treated COLO320DM cells using FISH with a biotinylated c-myc cosmid probe and FITC-avidin. Chromosomes were counterstained with propidium iodide (PI). (d, e) Asynchronously growing COLO320DM cells were directly fixed on chamber slides without colcemid treatment and processed for FISH analyses using c-myc cosmid probe. Clustered DMs (arrowheads) and segregating daughter chromosomes (PI stained) are indicated. Fluorescence images were collected using an epifluorescence microscope.

Figure 2

(A) Distribution of DMs to daughter cells visualized in living cells. Time lapse imaging of a H2B-GFP labeled COLO320DM cell from late anaphase to telophase. A cluster of lagging DMs (shown by arrowheads) formed a bridge between segregating chromosomes, and the bridge was severed by cytokinesis. Fluorescence images were collected every five minutes using an epifluorescence microscope equipped with a video camera. (B) A lagging DM cluster, separated from segregating normal chromosomes, forms a micronucleus (shown by arrowheads).

Figure 3

(A) Two color FISH analyses demonstrating the colocalization of lactose operator repeats with DMs. Digoxigenin labeled lactose operator DNA and biotinylated c-myc cosmid were used for hybridization. Signals were detected by rhodamine-conjugated anti-digoxigenin (for lactose operator: red) and FITC-avidin (for c-myc: green). Chromosomes were counter-stained with DAPI (blue).

(B) Two color FISH analyses using chromatin fibers prepared from the same cell line shown in (A). Note the arrays of lactose operator signals (red) and c-myc signals (green) on the same chromatin fiber (arrows). Chromatin fibers are counterstained with DAPI (blue).

Figure 4

Specific DM labeling using lactose operator/lactose repressor-GFP system.

Colon cancer cells harboring DMs with integrated lactose operator repeats were infected with a retrovirus expressing lactose repressor-GFP. Cells were fixed and chromosomes were counter-stained with DAPI (blue). DMs were visualized by specific binding of lactose-repressor-GFP fusion protein (yellow) to lactose operator repeats. Cells in interphase (a), prophase (b), and anaphase (c) of the cell cycle are shown.

References

1. Alitalo, K. & Shwab, M. (1986) *Adv Cancer Res* **47**, 235-281.
2. Bishop, M. (1991) *Cell* **64**, 235-248.
3. Wahl, G. M., Carroll, S. & Windle, B. (1992) in *Gene Amplification in Mammalian Cells: Techniques and Applications*, ed. Kellems, R., pp. 513-532.
4. Stark, G. R. & Wahl, G. M. (1984) *Ann Rev Biochem* **53**, 447-491.
5. Benner, S. E., Wahl, G. M. & Von Hoff, D. D. (1991) *Anti-Cancer Drugs* **2**, 11-25.
6. Von Hoff, D. D., McGill, J. R., Forseth, B. J., Davidson, K. K., Bradley, T. P., Van Devanter, D. R. & Wahl, G. M. (1992) *Proc Natl Acad Sci U S A* **89**, 8165-8169.
7. Shimizu, N., Kanda, T. & Wahl, G. M. (1996) *Nat Genet* **12**, 65-71.
8. Shimizu, N., Itoh, N., Utiyama, H. & Wahl, G. M. (1998) *J Cell Biol* **140**, 1307-20.

9. Von Hoff, D. D., Waddelow, T., Forseth, B., Davidson, K., Scott, J. & Wahl, G. M. (1991) *Cancer Research* **51**, 6273-6279.
10. Hollstein, M., Sidransky, D., Vogelstein, B. & Harris, C. C. (1991) *Science* **253**, 49-53.
11. Canute, G. W., Longo, S. L., Longo, J. A., Shetler, M. M., Coyle, T. E., Winfield, J. A. & Hahn, P. J. (1998) *Neurosurgery* **42**, 609-16.
12. Kanda, T., Sullivan, K. F. & Wahl, G. M. (1998) *Curr Biol* **8**, 377-85.
13. Alitalo, K., Schwab, M., Lin, C. C., Varmus, H. E. & Bishop, J. M. (1983) *Proc Natl Acad Sci U S A* **80**, 1707-1711.
14. Carroll, S. M., DeRose, M. L., Kolman, J. L., Nonet, G. H., Kelly, R. E. & Wahl, G. M. (1993) *Mol Cell Biol* **13**, 2971-81.
15. Levan, A. & Levan, G. (1978) *Hereditas* **88**, 81-92.
16. Robinett, C. C., Straight, A., Li, G., Willhelm, C., Sudlow, G., Murray, A. & Belmont, A. S. (1996) *J Cell Biol* **135**, 1685-1700.
17. Yates, J. L., Warren, N. & Sugden, B. (1985) *Nature* **313**, 812-5.
18. Parra, I. & Windle, B. (1993) *Nat Genet* **5**, 17-21.
19. Ellenberg, J., Siggia, E. D., Moreira, J. E., Smith, C. L., Presley, J. F., Worman, H. J. & Lippincott-Schwartz, J. (1997) *J Cell Biol* **138**, 1193-206.

Bibliography

1. Shimizu, N., Itoh, N., Utiyama, H. & Wahl, G. M. (1998) Selective entrapment of extrachromosomally amplified DNA by nuclear budding and micronucleation during S phase. *J Cell Biol* **140**, 1307-20.
2. Kanda, T., Sullivan, K. F. & Wahl, G. M. (1998) Histone-GFP fusion protein enables sensitive analysis of chromosome dynamics in living mammalian cells. *Curr Biol* **8**, 377-85. (data used for cover photograph).

Personnel supported by this grant:

1. Geoffrey M. Wahl, Ph.D., Principal Investigator
2. Teru Kanda, M.D., Ph.D., Post-doctoral fellow
3. Omid Vafa, Ph.D., Post-doctoral fellow

Figure 1

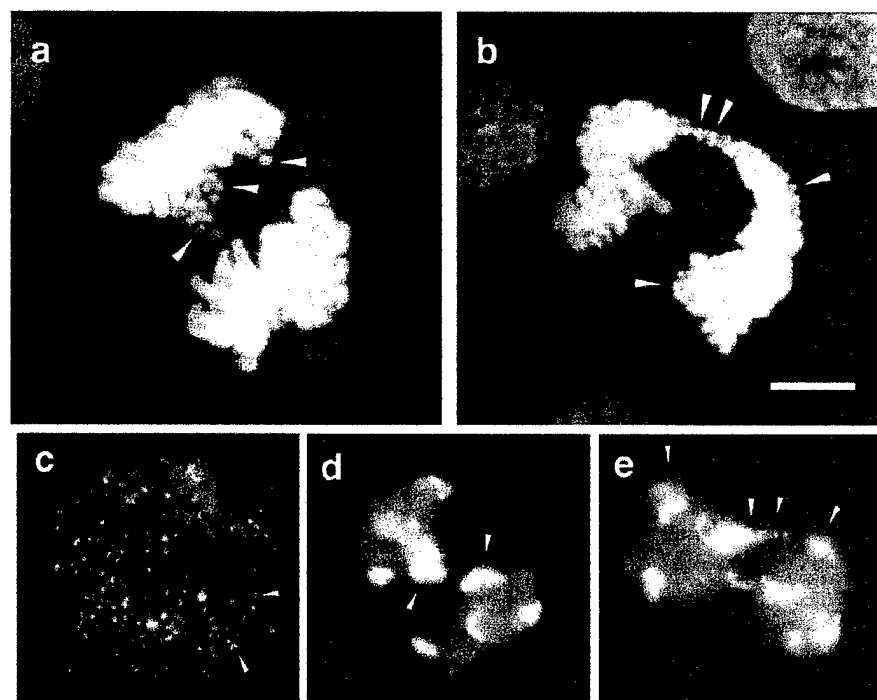
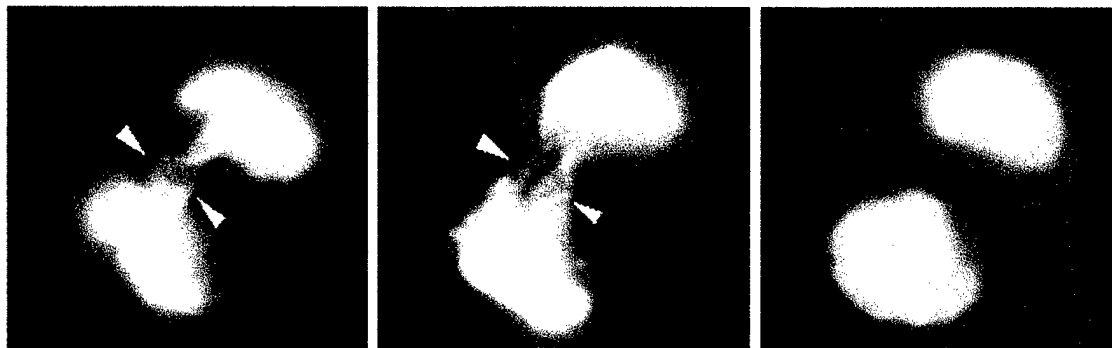


Figure 2

A



B



Figure 3A

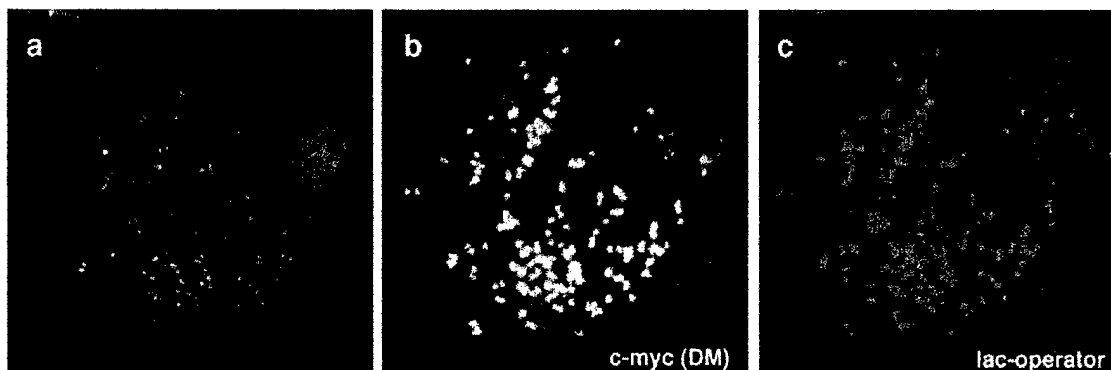


Figure 3B

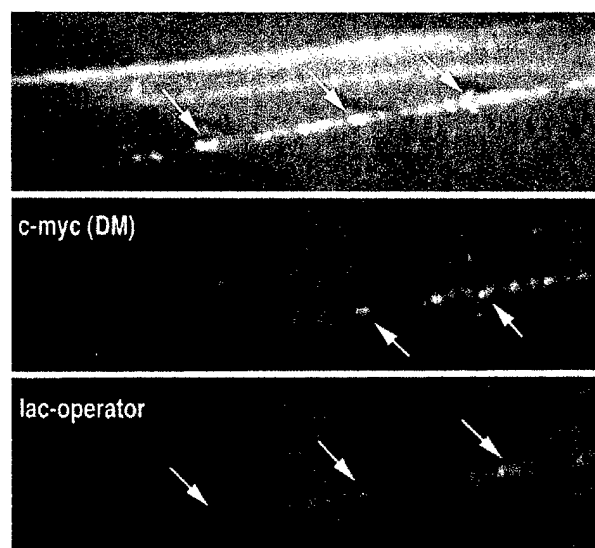
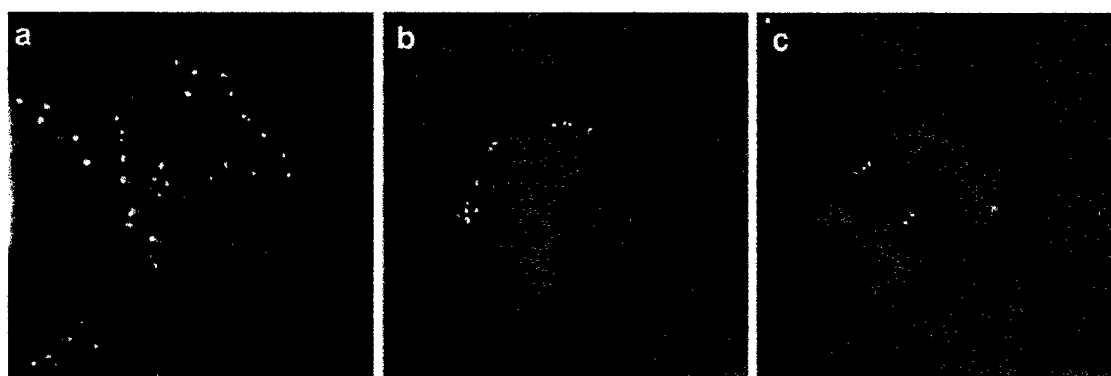


Figure 4



Selective Entrapment of Extrachromosomally Amplified DNA by Nuclear Budding and Micronucleation during S Phase

Noriaki Shimizu,* Nobuo Itoh,* Hiroyasu Utiyama,* and Geoffrey M. Wahl[‡]

*Faculty of Integrated Arts and Sciences, Hiroshima University, Higashi-Hiroshima, 724, Japan; and [‡]Gene Expression Laboratory, The Salk Institute for Biological Studies, La Jolla, California 92037

Abstract. Acentric, autonomously replicating extra-chromosomal structures called double-minute chromosomes (DMs) frequently mediate oncogene amplification in human tumors. We show that DMs can be removed from the nucleus by a novel micronucleation mechanism that is initiated by budding of the nuclear membrane during S phase. DMs containing *c-myc* oncogenes in a colon cancer cell line localized to and replicated at the nuclear periphery. Replication inhibitors increased micronucleation; cell synchronization and bromodeoxyuridine-pulse labeling demonstrated de

novo formation of buds and micronuclei during S phase. The frequencies of S-phase nuclear budding and micronucleation were increased dramatically in normal human cells by inactivating p53, suggesting that an S-phase function of p53 minimizes the probability of producing the broken chromosome fragments that induce budding and micronucleation. These data have implications for understanding the behavior of acentric DNA in interphase nuclei and for developing chemotherapeutic strategies based on this new mechanism for DM elimination.

THE accumulation of structural and numerical chromosome abnormalities in eukaryotic cells is limited by coordinating biosynthetic and repair processes with cell cycle checkpoints (Hartwell and Kastan, 1994). Mutations in genes involved in these transactions occur commonly during cancer progression and can greatly elevate the frequencies of base alterations or large-scale chromosome rearrangements. For example, defects in cell cycle-control pathways involving the p53 tumor suppressor gene create a permissive environment in which cells with aneuploidy, chromosome translocations, and gene amplification arise at high frequency in response to stresses created by antimetabolites or oncogene overexpression (Livingstone et al., 1992; Yin et al., 1992; Denko et al., 1994).

The types of aberrant chromosomal structures generated in cells with defective repair and cell cycle control functions are likely to be constrained by nuclear structure. For example, chromosomes with very long arms tend to generate nuclear projections variously referred to as "blebs" or "buds" (Ruddle, 1962; Lo and Fraccaro, 1974; Toledo et al., 1992; Pedoutour et al., 1994). A recent study in peas demonstrated that excessive DNA within a single chromosome arm generated a nuclear projection that was cut when the cell division plate formed after telophase

(Schubert and Oud, 1997). Sequences enclosed in such projections are often detected in micronuclei, suggesting that projections can be precursors of micronuclei (Toledo et al., 1992; Pedoutour et al., 1994), and that the chromosomal sequences they contain can be lost from the nucleus. These data indicate that a maximum allowable size exists for each chromosome arm within the nuclei of specific cell types.

Circular, autonomously replicating DNA fragments such as double-minute chromosomes (DMs)¹ are also frequently generated in cancer cells (Barker, 1982; Cowell, 1982; Bénner et al., 1991). These structures encode proteins that provide survival advantages *in vivo*, or resistance to a variety of chemotherapeutic agents *in vitro* (Alitalo and Shwab, 1986; Wahl, 1989; Von Hoff et al., 1992; Brison, 1993; Shimizu et al., 1994; Eckhardt et al., 1994). DMs replicate using cellular replication origins (Carroll et al., 1993), but lacking centromeres, they do not segregate by the same mechanisms used by chromosomes. Consequently, DMs are lost spontaneously in the absence of selection. Drugs such as hydroxyurea (HU) significantly increase the loss rate of DMs in human and rodent cell lines (Snapka and Varshavsky, 1983; Von Hoff et al., 1991; Von

Address all correspondence to Geoffrey Wahl, Gene Expression Laboratory, The Salk Institute, 10010 North Torrey Pines Road, La Jolla, CA 92037. Tel: (619) 453-4100. Fax: (619) 552-8285. E-mail: wahl@salk.edu

1. *Abbreviations used in this paper:* BrdU, 5-bromo-2'-deoxyuridine; DAPI, 4'-6-diamidino-2-phenylindole; DM, double-minute chromosome(s); FISH, fluorescence in situ hybridization; HU, hydroxyurea; PALA, *N*-phosphoracetyl-L-aspartate; PFA, paraformaldehyde; PI, propidium iodide; RPE-h, normal human retinal pigmented epithelial cells.

Hoff et al., 1992; Eckhardt et al., 1994; Canute et al., 1996). DM elimination results in increased drug sensitivity, reduced tumorigenicity, or differentiation, depending on the proteins expressed by DM-encoded genes (Snapka and Varshavsky, 1983; Snapka, 1992; Von Hoff et al., 1992; Eckhardt et al., 1994; Shimizu et al., 1994). Identifying the mechanisms by which DMs are eliminated could enable the development of new and more selective chemotherapeutic strategies, since DMs are uniquely found in cancer cells, and chromosome loss should not be induced by such treatments.

Like abnormally long chromosome arms, DMs have also been reported to be preferentially incorporated within micronuclei that are removed from the cell (Von Hoff et al., 1992; Shimizu et al., 1996). It is clear that small size alone does not guarantee selective enclosure of DNA fragments within micronuclei because a centric minichromosome the size of a typical DM is effectively excluded from micronuclei (Shimizu et al., 1996). This observation is consistent with the classical mechanism of micronucleus formation that involves the enclosure of lagging acentric chromosome fragments as nuclear membranes reform at the end of mitosis (Heddle and Carrano, 1977; Heddle et al., 1983). Thus, one would expect postmitotic enclosure of DMs within micronuclei since they typically lack functional centromeres (Levan et al., 1976). However, DMs appear to associate with chromosomes or nucleoli, which may enable most of them to evade such a postmitotic mechanism. The ability of DMs to "hitchhike" by association with mitotic chromosomes or nucleoli provides one explanation of why few micronuclei were detected at the midbody in a cell line containing numerous DMs (Levan and Levan, 1978), and their surprisingly efficient partitioning to daughter cells in some cell lines (Levan and Levan, 1978; Hamkalo et al., 1985). However, the interphase behavior of normal chromosomes and DMs may differ because DMs lack the centromeres and/or telomeres that position chromosomes in restricted territories and produce a choreographed set of chromosome movements during S phase (DeBonis and Mintz, 1986; Cremer et al., 1993). It has neither been determined whether acentric DM-DNA occupies positions different from chromosomes in interphase, nor whether this could enable their removal from the nucleus by a budding process like that observed for abnormally long chromosomes (Ruddle, 1962; Jackson and Clement, 1974; Lo and Fraccaro, 1974; Miele et al., 1989; Toledo et al., 1992).

DMs provide an excellent model for analyzing the nuclear behavior of multimegabase replicons lacking a centromere and telomeres. We show that DMs can preferentially localize the nuclear periphery, whereas chromosomally amplified sequences occupy a more central position. Although the micronuclei that entrap acentric chromosome fragments have typically been viewed to be generated postmitotically, we provide evidence for a novel micronucleation mechanism that involves the formation of nuclear projections which we refer to as buds. Buds form during S phase and appear to selectively associate with DMs replicating near or at the nuclear periphery. Since micronuclei are indicators of DNA damage and are produced at much higher frequencies in tumor cells than in normal cells, we investigated whether micronucleation frequency is increased in cells with defects in cellular responses to DNA

damage. We show that loss of p53 function increases the frequency of micronucleation and enables buds and micronuclei to be produced under conditions expected to lead to chromosome breakage.

Materials and Methods

Cell Culture

Human COLO 320DM (CCL 220) and COLO 320HSR (CCL 220.1) neuroendocrine tumor cells were obtained from American Type Culture Collection (Rockville, MD) and then single cell subclones were obtained by limiting dilution (Von Hoff et al., 1988). The locations of amplified *c-myc* genes to DMs or HSRs were confirmed by fluorescence in situ hybridization (FISH) using *c-myc* cosmid DNA. The cells were grown in RPMI 1640 medium supplemented with 10% FBS. The WS1 human embryonic skin fibroblast, obtained from American Type Culture Collection (CRL 1502), was cultured in DME supplemented with 10% heat-inactivated, dialyzed FBS, and $1 \times$ MEM nonessential amino acids. WS1-neo and WS1-E6 were kind gifts of S. Linke (National Institutes of Health, Bethesda, MD), and were generated by infecting WS1 with retroviral vectors expressing genes encoding either neomycin resistance or both neomycin resistance and the E6 protein from human papilloma virus 16, respectively (Linke et al., 1996). RPE-h (normal human retinal pigmented epithelial cells) and its neo and E6 derivatives were also kindly provided by S. Linke and the parental cells were obtained from Cell Genesys, Inc. (Foster City, CA). Epithelial cells were cultured in the same way as WS1.

Chemicals

Aphidicolin, 5-bromo-2'-deoxyuridine (BrdU), coumarin (1, 2-benzopyrone), deferrioxamine mesylate (desferrioxamine mesylate), DMSO, hydroxyurea, nicotinamide, thymidine, and nocodazole (methyl-[5-[2-thienylcarbonyl]-1H-benzimidazol-2-yl]carbamate) were obtained from Sigma Chemical Co. (St. Louis, MO). Guanazole (3,5-diamino-1,2,4-triazole) was from Aldrich Chemical Co. (Milwaukee, WI). PALA (*N*-phosphonacetyl-L-aspartate) was provided by the Drug Biosynthesis and Chemistry Branch, Developmental Therapeutics Program, Division of Cancer Treatment, National Cancer Institute (Bethesda, MD).

Cell Cycle Analysis

Cell cycle distribution was analyzed using flow cytometry as described previously (Yin et al., 1992; Di Leonardo et al., 1994). Cells treated with the indicated concentrations of drugs for the indicated times were labeled with $10 \mu\text{M}$ BrdU for 30 min. The cells were collected, fixed with 70% ethanol, treated with 0.1 N HCl containing 0.5% Triton X-100 (Mallinckrodt, Paris, KY), and then followed by boiling for 10 min and rapid cooling to denature the DNA. The nuclei were then incubated with FITC-conjugated anti-BrdU antibodies (Boehringer Mannheim Biochemicals, Indianapolis, IN) and counterstained with $2 \mu\text{g/ml}$ of propidium iodide (PI) containing RNase ($200 \mu\text{g/ml}$). Samples were analyzed using a Becton Dickinson FACScan™ (Sparks, MD). 10,000 events were collected for each sample. Data were analyzed using Sun Display as described previously (Yin et al., 1992; Di Leonardo et al., 1994).

Quantification of Micronuclei

Micronuclei containing DM sequences in COLO 320DM cells (see Figs. 2 and 3) were detected by preparing chromosome spreads using standard hypotonic swelling conditions (Lawce and Brown, 1991), followed by hybridization with a biotinylated *c-myc* cosmid probe as described previously (Shimizu et al., 1996). Total micronuclei (see Fig. 3) were determined by staining chromosome spreads with 4',6-diamidino-2-phenylindole (DAPI) (Sigma Chemical Co.; $1 \mu\text{g/ml}$ in VectaShield, Vector Labs, Inc., Burlingame, CA). The adherent cells (WS1, RPE-h, and their derivatives) were grown on coverslips, fixed with cold acetone (-20°C for 5 min) followed by cold methanol (-20°C for 5 min), rehydrated with PBS, and then stained with DAPI ($1 \mu\text{g/ml}$ in VectaShield). The numbers of total or DM-enriched micronuclei were scored using 60 or $100\times$ objectives and a fluorescence microscope equipped with appropriate epifluorescence filters (model Zeiss WL; Carl Zeiss, Inc., Thornwood, NY). The results are expressed as *Frequency of Micronuclei (%)* relative to the number of interphase nuclei scored ($\geq 1,000$ for each point).

Cell Synchronization

Synchronization was performed as described previously (Stein et al., 1994). Rapidly growing COLO 320DM cells were first arrested in early S phase using excess thymidine (2 mM) for 17 h. The cells were then washed with growth medium, released into growth medium containing 25 μ M 2'-deoxycytidine for 12 h (to reverse thymidine toxicity), and then incubated in 2.5 μ g/ml aphidicolin for 17 h to arrest cells as they entered S phase. The arrested cells were washed with growth medium and then either released into medium lacking drug, or into medium containing nocodazole (0.4 μ g/ml). Cell cycle progression was monitored using incorporation of [3 H]thymidine (Stein et al., 1994). To monitor the progression through mitosis, a portion (1 ml) of culture was fixed by paraformaldehyde (PFA; 2%) and then stained with DAPI. The frequency of cells in mitosis was scored using fluorescence microscopy. WS1-E6 cells were synchronized by seeding them at low density in 15-cm dishes with or without coverslips (18 \times 18 mm). The day after subculture, the medium was removed and then replaced with medium containing 0.1% FCS, and then followed by the culture for an additional 48 h. Cells arrested at G0 by serum deprivation were released into growth medium containing 5 μ g/ml aphidicolin for 15 h to arrest them at the beginning of S phase. Cells were released into S phase by replacing the medium with fresh growth medium lacking drug. Progression into S phase was monitored by the incorporation of [3 H]thymidine (Stein et al., 1994). The number of cells that were in S phase just before release from synchrony was monitored by BrdU-pulse labeling (30 min) followed by confocal examination of the labeling pattern as described in the following section (see Simultaneous Determination of DM Location and DNA Replication Using FISH and BrdU Incorporation). Concurrently, coverslips were removed, fixed with acetone and methanol, stained by DAPI, and then the frequency of micronuclei, nuclear budding, and mitotic cells were scored as described above.

Terminal Deoxynucleotidyl Transferase-mediated dUTP-Biotin Nick-end Labeling Assay

Terminal deoxynucleotidyl transferase-mediated dUTP-biotin nick-end labeling (TUNEL) assay was done according to a previously published procedure (Gavrieli et al., 1992) modified as described below. In brief, COLO 320DM cells were fixed in 2% PFA (10 min at room temperature) and then centrifuged onto a glass slide using a cytospin (Salk Institute Shop) apparatus. The cells were further fixed in cold methanol (-20°C , 5 min) followed by cold acetone (-20°C , 5 min). The slides were rehydrated in PBS and then equilibrated in reaction buffer (200 mM sodium cacodylate, 1 mM MgCl_2 , 1 mM β -mercaptoethanol, pH 7.2) for 15 min at room temperature. The end-labeling reaction was done by incubating the slides with the reaction buffer containing 10 μ M biotin-dUTP (Boehringer Mannheim GmbH, Mannheim, Germany), and 0.3 U/ μ l of terminal deoxynucleotidyl transferase (Toyobo Co., Osaka, Japan), for 60 min at 37°C . The slides were washed extensively, blocked with 20% FCS, and then the incorporated biotin was detected using FITC-conjugated streptavidin as in the protocol for FISH (see below). The slides were treated with RNase A (100 μ g/ml, 37°C , for 20 min), counterstained with PI, and then observed under the conditions used for FISH.

Probe Preparation and FISH

Preparation of probe from purified micronuclei was as described (Shimizu et al., 1996), except that DNA in the purified micronuclei was directly used for biotin labeling by using the BioPrime DNA Labeling System (Life Technologies Inc., Gaithersburg, MD). C-myc cosmid DNA probe was prepared as described (Shimizu et al., 1996). FISH using standard methanol/acetic acid-fixed nuclei was performed as described previously (Shimizu et al., 1996). Assessments of DM localization by confocal microscopy required the following procedure to preserve the spherical shape of the nuclei. This protocol, based on that developed for human lymphocytes (Ferguson and Ward, 1992; Vourc'h et al., 1993), could not be applied directly to COLO 320DM due to severe nuclear aggregation. The modified procedure involves pelleting 10 ml of COLO 320DM cells by centrifugation at 260 g for 5 min, followed by complete removal of the supernatant. The cells were gently suspended in 50 μ l of growth medium and then 10 ml of prewarmed (37°C) 75 mM KCl, 2 mM CaCl_2 was added slowly. The suspension was centrifuged immediately as described above and the supernatant was removed completely. The cell pellet was loosened gently, suspended in 1 ml of 75 mM KCl and 2 mM CaCl_2 at 4°C , and then followed by addition of 1 ml of 75 mM KCl, 2 mM CaCl_2 , 0.5% Triton X-100

at 4°C . The suspension was kept on ice for 10 min, then Dounce homogenized (loose fitting pestle, 5 times, at 4°C ; Fisher, Pittsburgh, PA). 1.5 vol of 5% PFA in PBS was added to the suspension and then incubated for 10 min at room temperature with occasional gentle shaking. After incubation, a 1:10 vol of 1 M Tris-HCl, pH 7.4, containing 1% BSA was added and further incubated for 10 min at room temperature with gentle shaking. The fixed nuclei were washed twice with PBS containing 1% FCS and then stored at 4°C up to 1 wk. Before FISH hybridization, the fixed nuclei were sedimented by cytospin onto poly L-lysine-coated glass slides (Matsunami Glass Ind., Ltd., Osaka, Japan). Slides were treated with RNase A (Sigma Chemical Co., 100 μ g/ml in 2 \times SSC, 37°C for 60 min), washed once with 2 \times SSC for 3 min, and then followed by blocking with 3% BSA in PBS for 30 min at 37°C . Slides were incubated in 50% formamide dissolved in 2 \times SSC for 30 min at room temperature to enable buffer equilibration, followed by addition of the hybridization mixture containing labeled probe (prepared as for standard FISH [Shimizu et al., 1996]). The sample was covered by a coverslip, sealed completely with rubber cement, denatured at 85°C , and then hybridized using overnight incubation at 37°C . Washing and the detection of the hybridized probe were performed as described previously (Shimizu et al., 1996). In some cases, intact cells were fixed directly and then hybridized. For this purpose, the cells were cytocentrifuged onto poly L-lysine-coated slides, fixed with ethanol/acetic acid (19:1) for 3 min at -20°C , rehydrated with PBS, and then treated with 4% formaldehyde in PBS for 10 min at 4°C . The slides were then washed extensively with PBS and hybridized as described above for isolated nuclei. Images were obtained using a Bio-Rad MRC600 confocal system (Hercules, CA) on a Zeiss Axiovert 135 microscope (see Fig. 6). Most images were obtained using a 63 \times objective (Apochromat, 1.40, oil, Carl Zeiss, Inc.), and zoom factor two. The acquired digital images were expressed as pseudocolors and then merged using Adobe Photoshop (Adobe Systems Inc., Mountain View, CA).

Localizing DMs in Interphase Nuclei

The locations of DMs in confocal nuclear sections were determined by measuring the distance from each of the hybridized signals to the center of the nucleus using the corresponding nuclear diameter as a unit length. Coplanar PI (DNA) and FITC (hybridized signal) images intercepting the center of the nucleus were obtained from randomly chosen nuclei. The digital images were merged using COMOS software (Bio-Rad Laboratories). The threshold value for each FITC signal was lowered until each signal, representing the domain of one or more DMs, became a single dot to enable accurate distance measurements. The distances from this dot to the center of the nucleus and the nuclear diameter were determined. The location of each signal in the nucleus was expressed by dividing the former number by the latter number. According to this expression, the center of the nucleus is 0, and the outer edge of the nuclear membrane is 1. At the same time, the intensity of each signal was measured using an arbitrary unit scale. These values were determined for every signal in each of the nuclear sections using a minimum of 100 randomly chosen nuclei for each sample. This procedure gives rise to a distribution of DM signals in each two-dimensional focal plane. The heights and widths of each nucleus were found to be approximately equal, indicating that the fixation procedure preserved a spherical nuclear morphology. We assume that the distribution of signals within each nuclear vol should correspond to the number of signals we detected at the corresponding radius in two-dimensional space. Therefore, we corrected the number of signals at each radial location to represent the number that should be present in the spherical volume corresponding to that radius.

Simultaneous Determination of DM Location and DNA Replication Using FISH and BrdU Incorporation

Rapidly growing COLO 320DM cultures were pulse labeled using 10 μ M BrdU (Sigma Chemical Co.) for 1 h and then followed by immediate cell collection. The pulse-labeling period was 30 min for the experiment presented in Fig. 2, G and H. The isolation of nuclei, fixation by PFA, and FISH using purified micronuclei probe were done as described above. After FISH, BrdU incorporation was determined by incubating the slides with anti-BrdU mouse monoclonal antibody (PharMingen, San Diego, CA) at a final concentration of 10 μ g/ml in PBS containing 0.1% BSA. After a 60-min incubation at 37°C , the slides were washed three times with PBS for 5 min each. The slides were then treated with rhodamine-labeled anti-mouse Ig (Boehringer Mannheim Biochemicals) at a final concentration of 10 μ g/ml in PBS containing 0.1% BSA. The slides were incubated

for 60 min at 37°C and then washed with PBS three times at 5 min each. The nuclei were viewed without counter staining, using an MRC 1024 (Bio-Rad Laboratories) confocal system equipped to Axiovert 135M microscope (Carl Zeiss, Inc.), and then the acquired digital images were processed as described above.

Results

Nuclear Budding during Interphase Can Selectively Entrap DMs

The classic mechanism by which acentric chromosome fragments such as DMs are lost from cells involves their enclosure within reforming nuclear membranes subsequent to telophase (for review see Heddle et al., 1991). However, there is one report that nuclear anomalies resembling micronuclei can be generated in interphase subsequent to γ irradiation (Duncan et al., 1985). We used a cell line with amplified *c-myc* genes to assess the relative contributions of postmitotic and interphase mechanisms to DM micronucleation.

A FISH analysis of COLO 320DM, a colon cancer cell line of neuroendocrine origin, is shown in Fig. 1. A biotinylated FISH probe specific for the *c-myc* amplicon in COLO 320 cells was obtained from micronuclei purified from COLO 320DM cells (Shimizu et al., 1996). FISH analysis with this probe showed that >95% of the cells in the

population contained only DMs, and the remainder contained DMs along with one intrachromosomally amplified region (Fig. 1 A, arrow). Consistent with a previous report (Levan and Levan, 1978), the DMs in the prometaphase spread (Fig. 1 A) do not appear to be distributed randomly since many localize to the periphery of the prometaphase ring. Peripheral nuclear localization was also observed in interphase nuclei using confocal microscopy (see below).

Analyses of exponentially growing cultures of COLO 320DM cells by a conventional FISH procedure revealed that $2.8 \pm 0.9\%$ of interphase nuclei have projections or buds. These buds can be classified into two types by FISH analysis using the probe described above. The first class ($56 \pm 12.2\%$ of the nuclear buds) contained highly concentrated DM sequences (Fig. 1, B–D show representative buds that contain DMs; C shows two micronuclei and one bud). We also observed a second class of buds that were stained with PI, but did not hybridize with the DM probe. This suggests that DNA that does not hybridize with the DM probe was contained in these buds. (see Discussion). However, the selectivity for acentromeric sequences such as DMs appears to be very high. This is indicated by the nuclear bud shown in Fig. 1 D that contains three DNA clusters that stain with PI (the red signal represents DNA staining as these samples were first treated extensively with RNase) and that hybridize intensely with the micro-

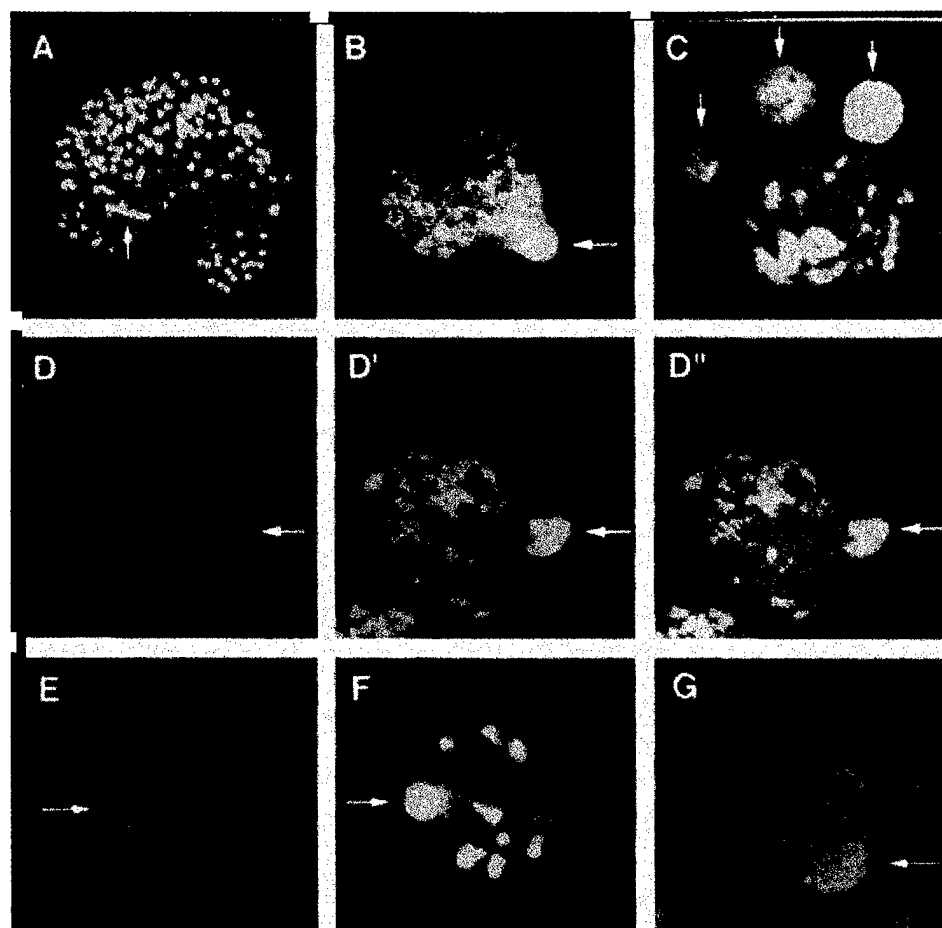


Figure 1. Nuclear budding selectively entraps DMs. Exponentially growing COLO 320DM cells were examined by a conventional FISH procedure that includes hypotonic treatment and fixation with methanol/acetic acid (3:1) (A–E). Alternatively, cells grown on slides were directly fixed with ethanol/acetic acid (19:1) followed by formaldehyde fixation (F and G). The slides were treated with RNase and hybridized with biotinylated DNA from purified micronuclei, except E, which was hybridized with biotinylated *c-myc* cosmid DNA. The hybridized probe was detected by FITC-conjugated streptavidin and then the DNA was counterstained with PI. (A) A prometaphase figure that shows both the specificity of the probe for DM painting and documents the peripheral location of DMs around the prometaphase chromosomes. One chromosomally integrated HSR region is indicated by an arrow. These DMs are selectively incorporated into the nuclear buds formed in the interphase nuclei (B–G, arrows). DM capture by buds appears to be very selective because the three dense PI-positive signals obvious in the nuclear bud (D) label intensely with the FITC–FISH probe (D'). (D'') The merged image.

nuclear DNA-FISH probe (Fig 1 *D'*; merge shown in *D''*). The selective inclusion of DMs into buds was also readily apparent when we used a FISH probe derived from a cosmid containing the *c-myc* gene. (Fig. 1 *E*), PFA-fixed nuclei isolated by a hypotonic method (see Fig. 6), or an isotonic method (data not shown). Furthermore, the selective inclusion of DM sequences into nuclear buds was also apparent in intact cells fixed directly by ethanol/acetic acid (19:1) followed by formaldehyde (Fig. 1, *F* and *G*). The apparent preferential inclusion of DM sequences in buds is reminiscent of our previous finding that DMs are highly enriched in micronuclei and that chromosomes or minichromosomes with functional centromeres are excluded from micronuclei (Von Hoff et al., 1992; Shimizu et al., 1996). These data suggest that buds are precursors of micronuclei.

Nuclear Buds and Micronuclei Are Formed during S Phase

The nuclei with buds exhibit a morphology typical of an interphase cell, not one in mitosis. Therefore, we determined the kinetics of formation of micronuclei and nuclear buds to ascertain whether these structures can be generated during S phase. COLO 320DM cells were synchronized at the G1/S boundary using a two-step procedure involving treatment with high thymidine concentration to arrest cells during S phase, release for 12 h to enable progression through and exit from S phase, and then incubation with the DNA polymerase inhibitor aphidicolin to arrest cells at the beginning of the next S phase (Stein et al., 1994). Removal of aphidicolin resulted in rapid entry into S phase with a peak of [³H]thymidine uptake at 4 and a peak of mitosis at 10 h, respectively (Fig. 2 *A*). The cells entered a second, less synchronous cycle ≤ 19 h after release. The synchronization level of the first S phase was further quantified by BrdU-pulse labeling followed by confocal microscopic examination of the nuclear labeling patterns. The labeling pattern progressed as reported previously (O'Keefe et al., 1992), with six readily distinguishable patterns (Fig. 2 *G*, Patterns 0–6). Examination of the arrested cells ($t = 0$) revealed that 96.1% of the cells did not incorporate label (Fig. 2 *H*, Pattern 0) but the remaining 3.9% of cells exhibited the pattern expected for

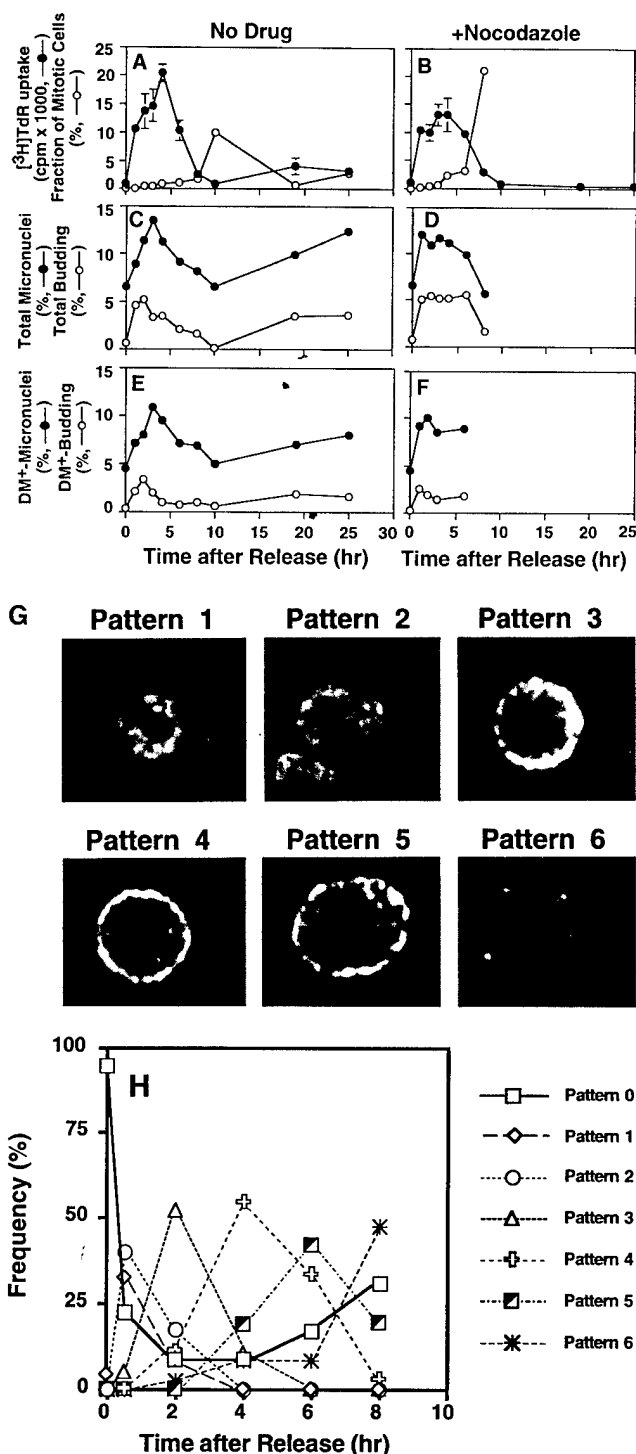


Figure 2. Formation of micronuclei and nuclear buds in a synchronized culture of COLO 320DM cells. COLO 320DM cells were synchronized at the G1/S boundary using a two-step procedure as described in Materials and Methods. The culture was divided into two portions and then released in the absence of any drug (*A*, *C*, and *E*), or the presence of 0.4 μ g/ml of nocodazole (*B*, *D*, and *F*). [³H]thymidine incorporation (closed circles) and the fraction of mitotic cells (open circles) were determined to monitor the synchronous progression through S and M phases, respectively (*A* and *B*). The numbers of total micronuclei (closed circles) and total nuclear buds (open circles) were determined in slides stained with DAPI (*C* and *D*). The numbers of DM+ micronuclei (closed circles) or DM+ nuclear buds (open circles) were determined in the slides hybridized with the purified micronuclei probe (*E* and *F*). These values are expressed as the frequency relative to the number of interphase nuclei scored (more than 1,000 for each point). The degree of synchronization was

further evaluated by pulse labeling the cells for 30 min with BrdU. At the times indicated, the cells were harvested and the incorporated BrdU was detected by anti-BrdU antibody and rhodamin-conjugated secondary antibody, and then examined by confocal microscopy. The distribution of BrdU labeling inside each nucleus was classified into 6 patterns (*G*); i.e., Pattern 0, no labeling; 1, only at the internal euchromatin; 2, spread of the labeling to periphery; 3, onset of labeling of peripheral heterochromatin; 4, almost exclusive labeling of peripheral heterochromatin; 5, labeling of peripheral and internal heterochromatin; and 6, exclusive labeling of internal heterochromatin. At each time point after release from aphidicolin block, the frequencies of each pattern scored from 100 nuclei were plotted (*H*).

early S phase (Fig. 2 *G*, Pattern 1). The small but significant fraction of cells in early S phase most likely reflects the leakiness of the synchronization procedure. After the release from the aphidicolin block, these patterns progressed sequentially as shown in Fig. 2, *G* and *H*. At the peak of [³H]thymidine uptake (4 h after release), 8.3% of cells still did not incorporate BrdU, suggesting that some cells may have been arrested irreversibly by aphidicolin.

The frequencies of micronuclei and buds were ascertained using the DNA specific dye DAPI (Fig. 2, *C* and *D*). We determined whether these structures contain amplified sequences by hybridizing all samples with the DM-painting probe obtained from micronuclei. The frequency of nuclei with buds at the G1/S boundary (i.e., $t = 0$) was nearly zero, increased dramatically as the cells progressed through early S phase ($t = 0-5$ h), declined in later S phase, and then gradually increased as the cells entered and progressed through a second S phase (Fig. 2 *C*). FISH analysis demonstrated that the buds enriched in DM sequences (DM + buds) showed the same time course (Fig. 2 *E*). The frequency of buds peaked concurrent with a BrdU labeling pattern characteristic of the onset of replication of peripheral heterochromatin (Fig. 2, *G* and *H*, Patterns 3). Importantly, the number of total micronuclei, or those with DMs, increased and declined in register with the number of nuclear buds (Fig. 2 *C*), suggesting that buds are precursors of micronuclei. We recently found that micronuclei containing DM sequences are released into the growth medium. The extracellular micronuclei were distinct from apoptotic bodies since they did not have condensed chromatin, the DNA was not degraded extensively, and the nuclear lamina were still intact (Shimizu, N., and G.M. Wahl, manuscript in preparation). Therefore, it is reasonable to propose that the decrease of micronuclei in late S phase reflects their release from the cells.

Whereas the frequency of nuclei with buds was low at the G1/S boundary, micronuclei were readily apparent (Fig. 2 *C*). One likely possibility is that these micronuclei were generated during the telophase of a previous cell cycle. We modified the synchronization strategy to include nocodazole to block cells in prometaphase after release from the aphidicolin block. This protocol restricts the analysis to micronuclei and buds generated within a single S phase, and to prevent buds or micronuclei produced from cells arrested before prometaphase of the previous cycle from entering the analysis (Cassimeris and Salmon, 1991). The treated cells entered and progressed through S phase at approximately the same rate as those not exposed to nocodazole (Fig. 2, compare *A* and *B*), and the mitotic index increased significantly by 8 h after release. The effectiveness of nocodazole treatment is also indicated by the inability of the drug-treated cells to progress into a second S phase over the time course used. Importantly, the number of nuclei with buds was again nearly zero at the G1/S boundary, and both the number of buds and micronuclei increased after release into nocodazole-containing medium. These data are consistent with the interpretation that nuclear buds and micronuclei can arise de novo during S-phase progression.

The kinetic and nuclear morphologic analyses of budding and micronucleation indicate that both events can occur during S phase. Since slowing replication fork progres-

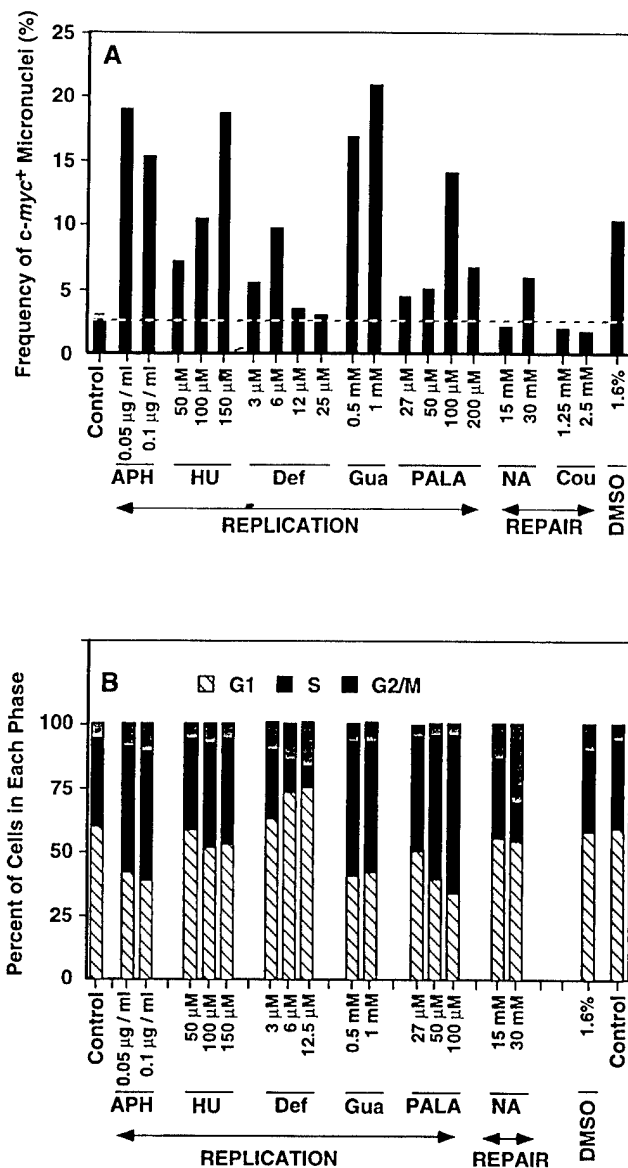


Figure 3. Effects of various drugs on induction of micronuclei and cell cycle distribution. COLO 320DM cells were treated for 3 d with inhibitors of DNA replication (APH, aphidicolin; Def, deferoxamine; Gua, guanazole; HU, hydroxyurea; and PALA), repair (Cou, coumarin; NA, nicotinamide) or the membrane-active agent DMSO at the concentrations indicated. (A) The treated cells were fixed with methanol/acetic acid and then hybridized with *c-myc* cosmid probe. The numbers of micronuclei that were stained brightly with *c-myc* probe were scored and expressed as frequency of *c-myc*⁺ micronuclei (%) relative to the number of interphase nuclei scored (more than 1,000 for each point). (B) The cells were pulse labeled with BrdU (for 30 min) at the end of the drug treatment and then analyzed by flow cytometry as described under Materials and Methods to determine the fraction of cells in G1, S, and G2/M.

sion may lead to DNA breakage (Eki et al., 1987; Linke et al., 1996), and micronuclei preferentially capture acentric fragments (Von Hoff et al., 1992; Shimizu et al., 1996), we determined whether replication inhibitors increase S phase micronucleation efficiency. The drugs tested included inhibitors of ribonucleotide reductase (HU, deferoxamine,

and guanazole), an inhibitor (PALA) of the carbamyl phosphate synthetase, dihydro-orotase, aspartate transcarbamylase (CAD) enzyme complex that catalyzes the first three steps of de novo pyrimidine biosynthesis, and aphidicolin. DNA synthesis inhibitors produced substantial increases in micronucleation, and this generally correlated with an increased fraction of cells in S phase (Fig. 3, A and B). A sharp decrease in micronucleation efficiency was observed for deferoxamine and PALA when these drugs were used at concentrations that severely inhibited S phase (Fig. 3 B and data not shown). These data indicate that micronucleation can result from inhibitors that retard replication fork progression and lengthen S phase.

We analyzed the effects of inhibitors that do not affect DNA synthesis to ascertain whether micronucleation can result from interfering with other DNA transactions such as DNA repair, or by interfering with membrane structure. Two inhibitors of poly(ADP-ribose) polymerase (nicotinamide and coumarin) were tested since ADP ribosylation has been implicated in DNA repair (Satoh and Lindahl, 1992), and inhibiting repair could increase the probability of generating acentric chromosome fragments. We tested the effects of DMSO, a membrane-active polar compound previously reported to reduce DM copy number in some tumor cell lines (Shima et al., 1989; Eckhardt et al., 1994). DMSO increased micronucleation without lengthening S phase (Fig. 3, A and B). Coumarin had no effect on micronucleation, whereas nicotinamide produced a small increase under conditions that apparently

increased the amount of damage in the cells since there was a significant increase in the G2 fraction (Fig. 3, A and B). These data are consistent with the view that micronucleation efficiency can be increased by at least two mechanisms, one of which presumably involves perturbing replication fork progression, and another of which may involve events occurring outside of S phase.

Peripheral Nuclear Localization of DMs Correlates with Their Elimination by Budding

Insight into the mechanisms underlying the selective inclusion of DMs into nuclear buds and the formation of these structures in interphase was obtained by confocal microscopy. PFA fixation of nuclei was used for optimal preservation of nuclear morphology (Manuelidis and Borden, 1988).

Confocal sections from three representative nuclei isolated from rapidly growing untreated COLO 320DM cells are shown in Fig. 4, A–C. FISH revealed preferential localization of most DM sequences to the nuclear periphery, as indicated by the significant hybridization intensity, clustering, and number of DM signals at the extreme edge of each nucleus. Note the substantial deviation from a random distribution of DM sequences at the nuclear periphery (quantified in Fig. 5 A by measuring DM positions relative to the center of each nucleus in 100 interphase nuclei). By contrast, sequences amplified within chromosomes in the closely related cell line COLO 320HSR

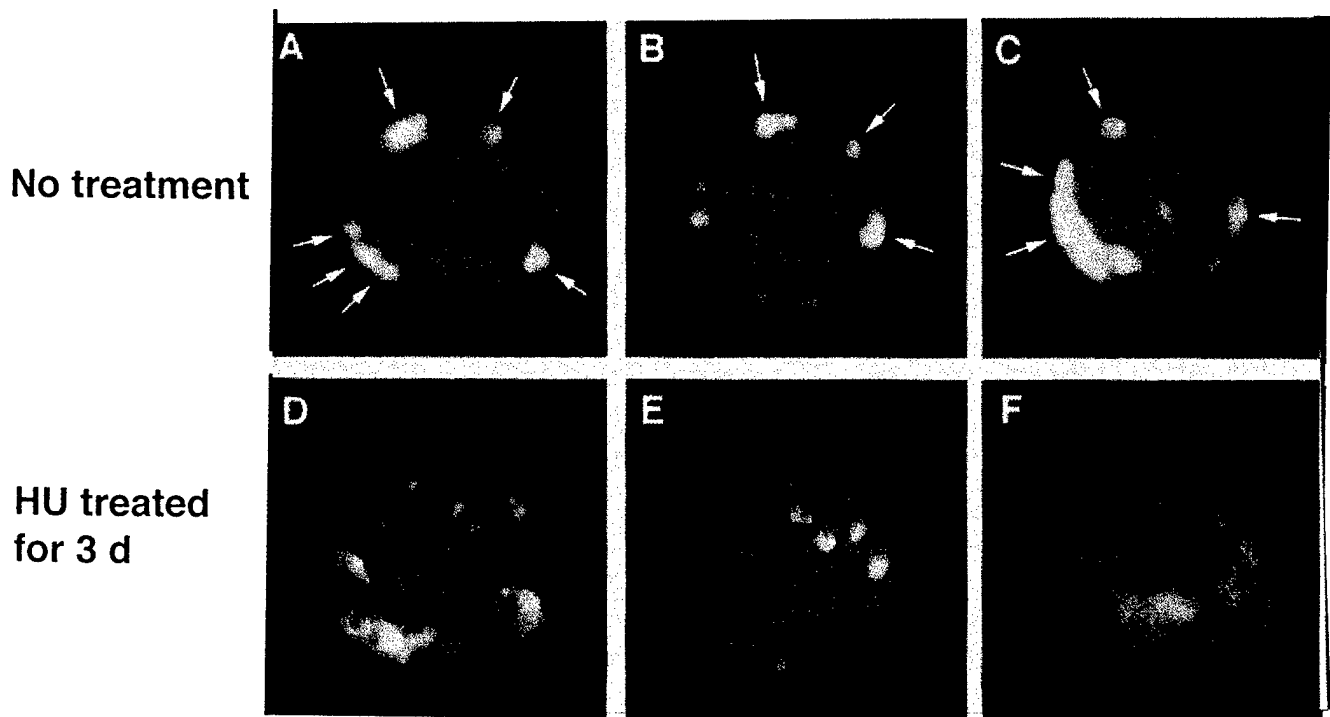


Figure 4. Localization of DMs in interphase COLO 320DM nuclei. PFA-fixed isolated nuclei from a culture of COLO 320DM cells were hybridized with a DM painting probe and then counterstained with PI. Optical sections near the center of each nucleus were obtained using confocal laser scanning microscopy. Each of three representative images of nuclei from the rapidly growing culture (A–C) and from a culture treated with 100 μ M HU for 3 d (D–F) are shown. In untreated cultures, DMs preferentially located just beneath the nuclear membrane as indicated by the arrows. Very few peripheral DMs were detected in the nuclei from the HU-treated culture, and most of the signals localized well within the nucleus as shown.

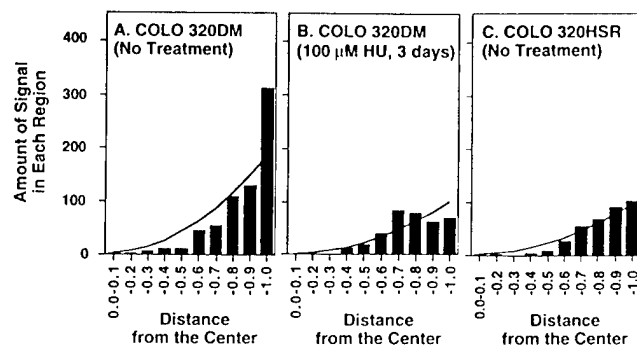


Figure 5. Quantitative analysis of the nuclear positions of DMs and chromosomally amplified sequences. The nuclei from a rapidly growing culture of COLO 320DM cells (A), COLO 320DM treated with 100 μ M HU for 3 d (B), and rapidly growing COLO 320 cells with chromosomally amplified *c-myc* sequences (COLO 320HSR) (C) were hybridized with a probe for the *c-myc* amplicon. Sections intercepting the center of each nucleus were obtained as in Fig. 4. For each section, the position and intensity of each hybridized signal was measured. Each analysis represents measurements on 100 randomly chosen nuclei. The abscissa depicts the fractional distance from the nuclear center (0, center; 1, periphery), and the ordinate is the number of signals detected at each position in 100 nuclei. The theoretical random distribution curves based on signals per nuclear vol at each position are shown in each graph as explained in greater detail in Materials and Methods.

showed a nearly random distribution throughout the nucleus (Fig. 5 C). HU treatment preferentially depleted DMs from the nuclear periphery (Fig. 4, D–F and Fig. 5 B, quantification) and then reduced the DM content per cell by approximately threefold as determined by competitive PCR amplification (for method see Shimizu et al., 1996; data not shown). Taken together with the data reported above, these results indicate that DM sequences located at the nuclear periphery are preferentially incorporated into nuclear buds, which are then removed from the nucleus through the formation of micronuclei.

Incorporation of Replicating DM Sequences into Nuclear Buds

The correlations between S phase progression, nuclear budding, and micronucleation reported above led us to investigate whether DM sequences undergoing replication are targeted for inclusion into buds. This possibility was examined by pulse labeling COLO 320DM cells with BrdU, and then hybridizing the isolated nuclei with the DM-FISH probe. Subsequent reaction with an anti-BrdU antibody and fluorescein-labeled secondary antibody enabled simultaneous detection of nuclei, buds, and micronuclei containing DMs that were undergoing DNA replication during the brief labeling interval. FISH analysis of two representative confocal sections (Fig. 6, A–A' and B–B') shows that nuclear buds in these cells (arrows) contain highly concentrated DM sequences. The nuclei, nuclear buds, and peripheral regions of each nucleus incorporated BrdU, indicating that these buds were formed in nuclei that were synthesizing DNA at the time of bud formation. Table I shows that BrdU+, DM+ buds (type I, I') represent 48% of the total population of DM-containing buds.

Some nuclei incorporated BrdU, but the buds they produced were not labeled (type 2, 2'; 35%). We infer that some of these buds were also generated during S phase (as opposed to during the previous cycle), and that they did not reveal BrdU incorporation because their DNA was not undergoing replication during the brief BrdU incubation period. Samples in which neither nuclei nor buds labeled with BrdU may represent examples where buds were generated outside of S phase (type 3; 17%). Alternatively, the presence of such buds (type 3) may indicate that these structures persist after DNA replication has finished, and may be sources of some of the micronuclei observed to form during mitosis. These data reveal a strong correlation between DMs undergoing replication and their inclusion in buds and micronuclei, and they lead to a conservative estimate of $\geq 50\%$ of the micronuclei produced during each cell cycle being generated during S phase.

The S phase micronucleation process described here superficially resembles the induction of "nuclear anomalies" by an apoptotic mechanism following γ irradiation (Duncan et al., 1985) or colchicine treatment (Duncan et al., 1984). However, the absence of highly condensed DNA in the nuclei-producing buds suggests that they were not undergoing apoptosis at the time of bud formation. To determine whether budding and micronucleation are separable from apoptosis, we determined whether buds contain the condensed, fragmented DNA that typifies apoptotic cells. Fragmented DNA was detected using the TUNEL assay in which terminal transferase is used to add BrdU to the 3'-OH groups generated by apoptotic DNA fragmentation (Gavrieli et al., 1992). The cells were also stained with PI to visualize all nuclei and buds. An example of the data obtained from such an analysis of COLO 320DM cells is shown in Fig. 6, C–C'. The TUNEL assay shows one cell with a lobular nucleus that exhibits a strong TUNEL reaction and typifies the fragmented, condensed DNA observed in apoptotic nuclei (Cohen, 1993). The PI staining in the middle panel reveals a cell producing a nuclear bud that does not stain by the TUNEL assay and does not exhibit the pycnotic structure of the apoptotic nucleus. Synchronization experiments showed that whereas $\sim 5\%$ of cells generated buds at the peak of S phase (e.g., refer to Fig. 2 C), only 0.5–1% were TUNEL positive. Other data (see Discussion) provide additional evidence that S phase budding and micronucleation do not require activation of an apoptotic program.

Micronucleation Occurs Infrequently in Normal Cells, and Is Increased upon p53 Inactivation

Micronucleation occurs at significantly lower rates in normal cells than tumor cell lines (Roser et al., 1989; Bondy et al., 1993). Since micronucleation can be induced by chromosome breakage (Heddle and Carrano, 1977), the observed increase in micronucleation in tumor cells might result from mutations that increase the probability of DNA breakage. The tumor suppressor p53 controls G1 arrest responses activated by DNA breakage and rNTP depletion induced by PALA treatment, and DNA breakage can occur in p53-deficient cell lines that enter S phase during PALA treatment (Livingstone et al., 1992; Yin et al., 1992; Linke et al., 1996). As reported above, PALA also induces

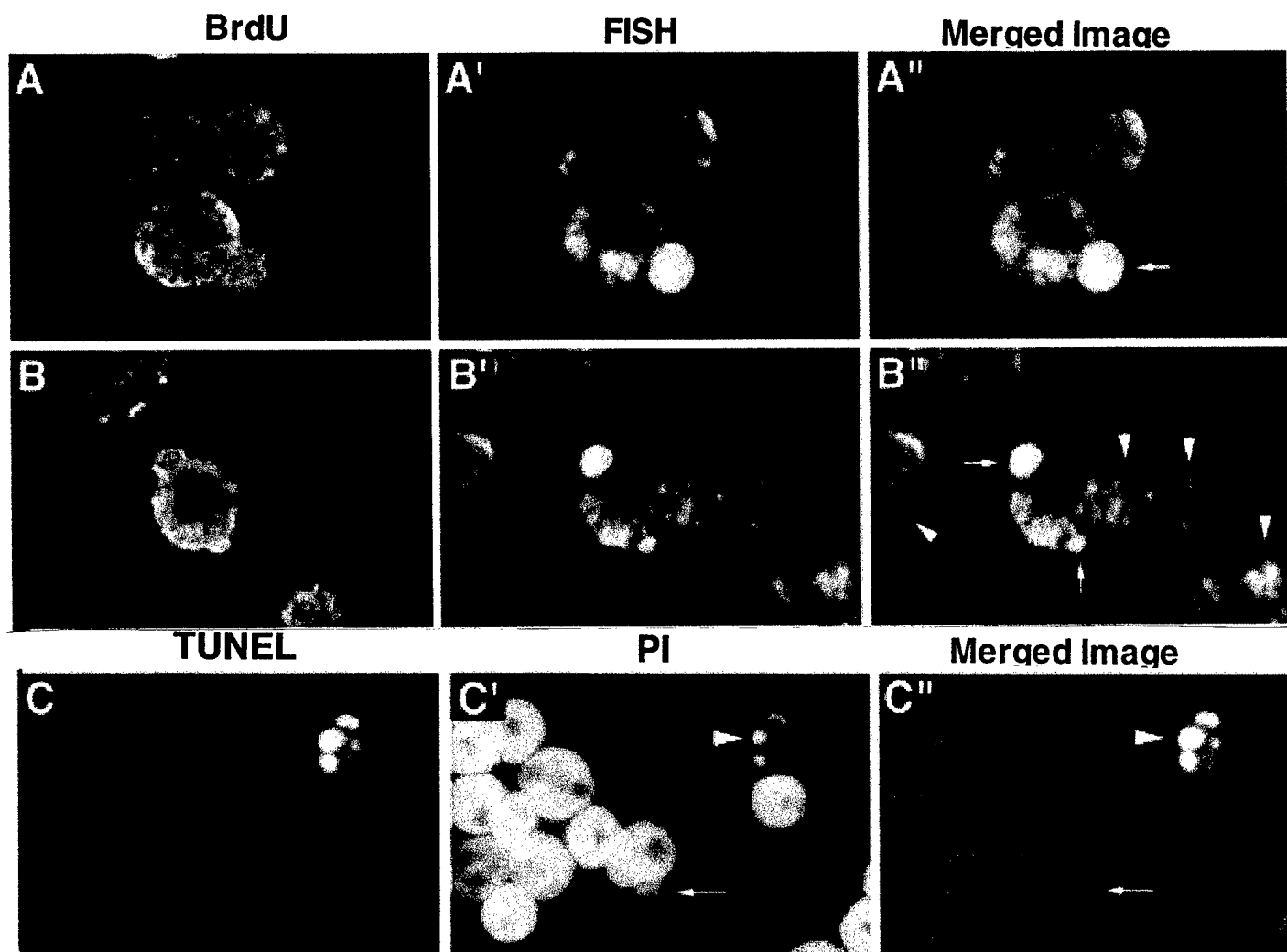


Figure 6. Analyses of DM-DNA replication and apoptosis in COLO 320DM cells. (A and B) A culture of rapidly growing COLO 320DM cells was pulse labeled with 10 μ M BrdU for 1 h. The nuclei were isolated, fixed with PFA, hybridized with the biotinylated DM painting probe, and then detected using FITC-conjugated streptavidin as in Fig. 4. Sites at which BrdU was incorporated were detected with an anti-BrdU mouse monoclonal antibody followed by rhodamine-conjugated anti-mouse immunoglobulin. The double-labeled nuclei were examined using a confocal laser scanning microscope. The images of BrdU, FISH, and the merged images (red, BrdU; green, FISH) are shown for two representative fields. Nuclear buds that selectively entrap DMs are indicated by *arrows*, and the cells that were not in S phase during the pulse label (BrdU-) are indicated by *arrowheads*. (C) Analysis of apoptosis in COLO 320DM cells was done using the TUNEL method as described in Materials and Methods. This representative photograph is from one experiment in which COLO 320DM cells were treated with 100 μ M HU for 3 d. The *arrow* points to a bud in a cell that is not undergoing apoptosis, whereas the *arrowhead* points to an apoptotic cell in the same field.

S-phase micronucleation in COLO 320 cells. These data led us to investigate whether p53 inactivation in normal diploid fibroblasts results in increased S-phase budding and micronucleation.

Human WS1 normal diploid fibroblasts, and two nearly isogenic derivatives generated by retroviral transduction of the neomycin phosphotransferase gene (WS1-neo) or an oncogenic derivative of the human papilloma virus E6 gene (WS1-E6) were used. The E6 gene product facilitates p53 degradation by a ubiquitin dependent pathway (Scheffner et al., 1990; Crook et al., 1991). Cell cycle checkpoint controls that regulate entry into S phase in the presence of DNA damage or limiting rNTP concentrations appear to be inactivated to equivalent degrees in human cells expressing mutant p53, oncogenic E6 protein, and mouse embryo fibroblasts with homozygous p53 knock out (Kastan

et al., 1992; Kuerbitz et al., 1992; Livingstone et al., 1992; Yin et al., 1992; White et al., 1994; Linke et al., 1996; Linke et al., 1997). Importantly, we previously showed that the frequency of γ radiation induced micronucleation is higher in p53-/- MEFs than in wild-type MEFs (Huang et al., 1996). It is likely, therefore, that effects on micronucleation observed upon expression of oncogenic E6 protein relate to inactivation of p53 rather than to other proteins that may be affected by E6.

The data shown in Fig. 7 demonstrate that E6 gene expression increases the micronucleation rate of WS1 cells. WS1 cells exhibit a low micronucleation rate that is not increased by HU or PALA (Fig. 7 A). Consistent with our previous studies (Linke et al., 1996), PALA induced a G1 cell cycle arrest, whereas HU did not significantly affect the percentage of WS1 cells in S phase at the concentra-

Table 1. Quantification of Budding and Micronucleation

Type	BrdU labeling in:		Frequency of DM+buds that belong to each type
	DM+buds	Nuclei	
1	+	+	26/60 (43%)
1'	±	+	3/60 (5%)
2	—	+	9/60 (15%)
2'	—	±	12/60 (20%)
3	—	—	10/60 (17%)

Nuclei from COLO 320DM were pulse labeled with BrdU and then analyzed for BrdU incorporation and DMs as described in Fig. 6. Nuclei were observed using epifluorescence microscopy. 60 nuclei with DM+buds were classified according to whether they labeled with BrdU (classes 1, 1'), whether the nuclei to which they were attached labeled with BrdU (classes 2, 2'), or whether neither bud nor nucleus labeled with BrdU (class 3). The number of nuclei belonging to each type were scored and expressed as nuclei in that class/total number scored.

tion used (Fig. 7 B). By contrast, E6 expression increased the micronucleation efficiency of these fibroblasts growing under normal conditions, and both HU and PALA produced a substantial further increase in micronucleation rate (Fig. 7 A), which correlated with a significant increase in the number of cells in S phase (Fig. 7 B). The importance of an E6 target, which we infer to be p53, in limiting micronucleation is evident in other cell types since similar results were obtained using RPE-h and their E6 expressing derivatives (data not shown).

The elongation of S phase and induction of micronuclei by HU and PALA in both COLO 320DM and WS1-E6 cells led us to assess whether budding in S phase is the predominant mechanism of micronucleation in WS1-E6 cells. WS1-neo and WS1-E6 cells were arrested in G0 by serum deprivation and then released in the presence of aphidicolin to arrest the cells at the G1/S boundary (Fig. 7 C). Synchronization by serum depletion did not increase mi-

cronucleation rate (data not shown) and then the micronucleation and budding frequencies did not increase in S phase in WS1-neo cells (Fig. 7 D). By contrast, removal of aphidicolin from WS1-E6 cells resulted in significant increases in the frequencies of both nuclear budding and micronucleation as the cells progressed through S phase (Fig. 7 D). Since DNA damage does not induce apoptosis in either WS1 or WS1-E6 cells (Di Leonardo et al., 1994; Linke et al., 1996; Linke et al., 1997), the increased S-phase micronucleation observed in these cells occurs independent of an apoptotic program.

Discussion

Loss of cell cycle checkpoints during cancer progression creates a permissive environment for the initiation and propagation of chromosomal rearrangements such as amplification of cellular protooncogenes. The persistence or elimination of these structures within the nucleus can, respectively, promote or inhibit cancer progression. Interestingly, in human tumors analyzed at biopsy, oncogene amplification occurs most frequently in acentric chromosomal fragments such as DMs (Benner et al., 1991), and micronucleation represents a major pathway for the elimination of such structures (Von Hoff et al., 1992; Shimizu et al., 1996). Before this report, micronucleation had been considered to result from imperfect segregation of acentric chromosomal fragments or fragments of overly long chromosomes during karyokinesis (Heddle and Carrano, 1977; Heddle et al., 1983). The results presented here, by contrast, reveal that acentric DMs are sorted to the nuclear periphery during S phase, and are then selectively eliminated from the nucleus by micronucleation in advance of karyokinesis.

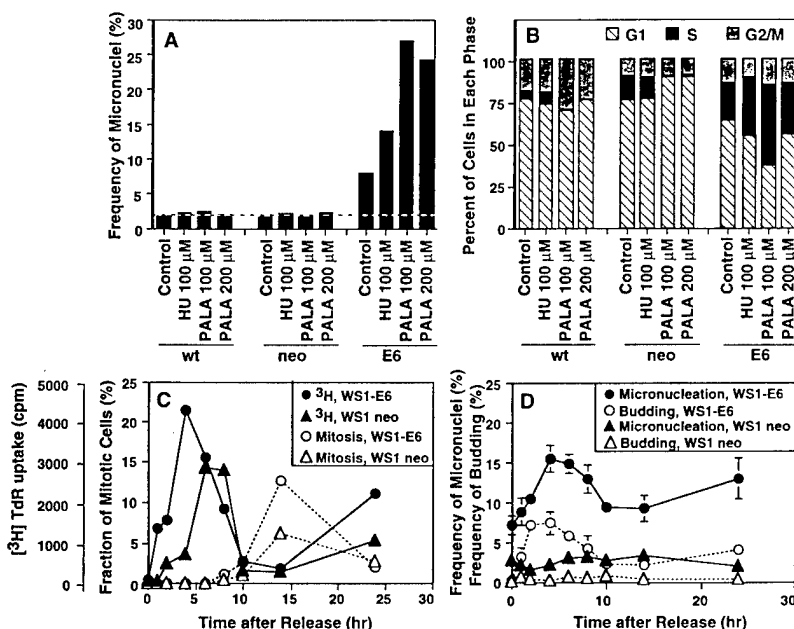


Figure 7. p53 deficiency increases S-phase budding and micronucleation in normal human diploid fibroblasts. Wild-type (wt) WS1 human diploid fibroblasts, or transformants expressing the neomycin resistance gene (*neo*) or both *neo* and the human papilloma virus E6 protein (*E6*) were generated by retroviral transduction. These cells were cultured in the absence or the presence of HU or PALA at the indicated concentrations for 3 d. (A) Cells grown on coverslips and treated as above, fixed, and then stained by DAPI. The number of micronuclei were scored and expressed as the frequency of micronuclei (%) relative to the number of interphase nuclei scored (more than 1,000 for each point). (B) Cell cycle effects of these drugs were examined as in Fig. 2 B. (C and D) The culture of WS1-neo (open and closed triangles) or WS1-E6 (open and closed circles) were synchronized at the G1/S boundary by the procedure described in Materials and Methods, and were released into growth medium. (C) Progression through S or M phase was monitored by the incorporation of [³H]thymidine (closed symbols) or the fraction of mitotic cells (open symbols). (D) The cells on the coverslips were fixed, stained with DAPI, and then the frequencies of micronuclei relative to the number of interphase nuclei were scored. >500 nuclei were counted for each point and the results are expressed as mean ± SD for WS1-neo and WS1-E6 cells (three independent determinations for each strain; error bars for WS1-neo data points were smaller than the sizes of the symbols). Nuclear budding frequencies were determined on the same slides as used to determine the micronucleation index (more than 1,000 nuclei for each point).

determined by microscopic detection of metaphase figures (open symbols). (D) The cells on the coverslips were fixed, stained with DAPI, and then the frequencies of micronuclei relative to the number of interphase nuclei were scored. >500 nuclei were counted for each point and the results are expressed as mean ± SD for WS1-neo and WS1-E6 cells (three independent determinations for each strain; error bars for WS1-neo data points were smaller than the sizes of the symbols). Nuclear budding frequencies were determined on the same slides as used to determine the micronucleation index (more than 1,000 nuclei for each point).

S Phase Budding and Micronucleation May Be the Predominant Mechanism for DM Elimination

We infer that S-phase micronucleation is a general characteristic of human cells with an aberrant p53 pathway since this process was observed in a human tumor cell line, and p53-deficient normal human fibroblasts and epithelial cells. The cell synchrony and release experiments provide direct evidence that budding begins as cells enter S phase. The experiment summarized in Table I shows that BrdU+ micronuclei account for almost 50% of the total micronuclei generated during a single S-phase. It is reasonable to infer that a fraction of the 35% of BrdU- micronuclei derived from BrdU+ nuclei did not incorporate the label because their DNA did not replicate during the brief BrdU pulse used. Such micronuclei would, therefore, also have originated during S phase, but we have no means of providing a precise estimate of this fraction. The available data do, however, demonstrate that S-phase micronucleation mediated by budding is at least as common as the classic postmitotic process, and may be the predominant mechanism for removing DMs from human cancer cells.

The parallel increases in budding and micronucleation frequencies as cells enter and proceed through S phase, and the absence of a significant temporal lag between the two, is consistent with a precursor-product relationship in which a micronucleus is produced shortly after a bud is generated. The decrease in budding and micronucleation during the latter part of S phase is also consistent with a tight linkage to the replication program, and suggests that once micronuclei are generated during S phase, some may be released from the cell, whereas others may fuse to nuclei or be degraded intracellularly. Among these possibilities, we have direct experimental evidence that some micronuclei may be expelled from the cell through the cytoplasmic membrane since we have observed extracellular micronuclei containing three membranes and amplified *c-myc* genes (Fig. 8; Shimizu, N., and G.M. Wahl, unpublished data). We are currently testing whether such micronuclei are bound by a cytoplasmic membrane, and whether they can fuse to the same or other cells in the population (Fig. 8).

The baseline frequency of micronuclei observed in cultures at the beginning of S phase in which budding was not yet evident suggests that some micronuclei were generated in a previous cycle and persisted for an extended time, which would be consistent with previous reports of long lived micronuclei (Heddle et al., 1983). It is conceivable, therefore, that there are two classes of micronuclei that differ from each other by their stability, perhaps because of structural distinctions deriving from their mechanisms of formation. Consistent with the inference of multiple types of micronuclei, we found that micronuclei can differ in their lamin and nuclear pore contents (Shimizu, N., and G. Wahl, unpublished observations). Experiments in progress are designed to elucidate whether such differences correlate with stability and alternative mechanisms of formation.

S-phase Budding and Micronucleation Do Not Require Previous Engagement of an Apoptotic Program, but Can Result in Apoptosis

Apoptosis can generate nuclear blebs (Dini et al., 1996)

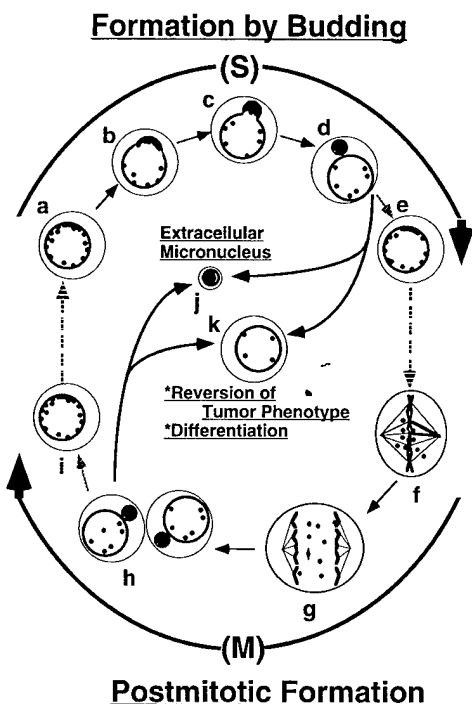


Figure 8. Model for the formation of micronuclei. Models for DM elimination by budding and micronucleation in S-phase and postmitotic micronucleation are shown. In the S-phase budding mechanism, DMs are preferentially located at the periphery of the interphase nucleus and then selectively encapsulated into nuclear buds that then pinch off to form micronuclei during DNA replication (a-d). This process is an alternative to the classical postmitotic mechanism of generating micronuclei depicted in f-h. One possible fate of these micronuclei is that they refuse to the main nucleus (i to j and d to e). At present, this is a speculation as there is no direct experimental evidence to support it. On the other hand, we do have direct evidence that micronuclei can be released into the culture supernatant as extracellular micronuclei, suggesting that they may be extruded through the cell membrane (j; Shimizu, N., and G.M. Wahl, unpublished data). Decrease in DM content can be achieved by either expulsion of micronuclei containing DMs from the cell, or by degradation of DM-DNA within intracellular micronuclei. In either case, loss of DM sequences from the nucleus results in reversion of the tumor phenotype, differentiation, or apoptosis (k; Von Hoff et al., 1992; Eckhardt et al., 1994; Shimizu et al., 1994).

and has been inferred to produce "nuclear anomalies" that resemble micronuclei (Duncan and Heddle, 1984; Duncan et al., 1985). However, our analyses show that nuclei that produced buds were not pycnotic and fragmented like apoptotic nuclei. Buds and micronuclei generated in COLO 320DM cells within a single S phase were not TUNEL positive, indicating that they did not contain fragmented DNA. Whereas apoptotic cells did arise in HU-treated COLO 320DM cultures, this required prolonged incubation, and occurred after a substantial fraction of the amplified *c-myc* genes had been removed. Furthermore, cells undergoing budding and micronucleation survived for several days, which is not expected if an apoptotic program were activated before micronucleation. A time course experiment similar to that described above (e.g., Fig. 2) revealed that budding increases during a single S phase whereas the fraction of cells undergoing apoptosis

remained roughly constant, and that most of those generating buds were not TUNEL positive (data not shown). Finally, though we have not observed apoptosis in normal fibroblasts (Di Leonardo et al., 1994), and loss of p53 function typically makes cells more resistant to apoptosis induced by growth conditions that can lead to DNA damage (White, 1994), S-phase budding and micronucleation were induced in normal diploid fibroblasts upon expression of oncogenic papillomavirus E6 protein, presumably due to elimination of p53 function. These observations lead us to propose that buds and micronuclei in COLO 320DM and WS1-E6 cells are produced by a mechanism that does not require prior engagement of the apoptotic program.

Mechanisms of Budding and Micronucleation

The molecular basis for inclusion of DMs in buds and micronuclei, and exclusion of similarly sized centric fragments from such structures (Shimizu et al., 1996), remains to be elucidated. We offer two potential explanations. The first relates to replication of DMs at an inappropriate nuclear location. Previous studies showed that heterochromatic DNA, such as that comprising inactive X chromosome-Barr bodies, typically replicates late in S phase at the nuclear periphery and is often enclosed within micronuclei, whereas the active X replicates earlier in S phase at a more internal position and is not subject to micronucleation (Dyer et al., 1989; Tucker et al., 1996). DMs are euchromatic and tend to replicate early in S phase, typically at approximately the same time as the native chromosomal locus (Carroll et al., 1991, 1993). However, as shown here, they can localize to and replicate at the nuclear periphery. Since chromosomes occupy specific territories within interphase nuclei (Cremer et al., 1993), the independence of DMs from chromosomes may prevent them from occupying the correct nuclear position and could explain their localization to the periphery. Peripheral localization may be a default position reflecting the inability of DMs to undergo the nuclear movements choreographed by centromeres and/or telomeres during S phase (DeBoni and Mintz, 1986; Ferguson and Ward, 1992; Vourc'h et al., 1993). Replication at such peripheral locations, or perhaps inability to move away from such sites into protected inner nuclear regions following replication, may then precipitate bud formation. A second explanation is that some chromosomal sequences may bind proteins that target the protein and associated nucleic acid to a particular nuclear location, such as the periphery. In the absence of a centromere/telomere, this protein-nucleic acid complex may be destined to form a nuclear bud until membrane fusion produces a micronucleus. This view is supported by recent studies in *Tetrahymena* demonstrating that *cis*-acting heterochromatic regions bound by the chromodomain protein Pdd1p are targeted to the nuclear periphery when the DNA is fragmented during macronuclear development (Madireddi et al., 1996). The peripheral, Pdd1p-associated acentric chromosomal fragments are then removed from the nucleus via micronucleation. The striking similarities between the observations in *Tetrahymena* and those reported here raise the intriguing possibility of an evolutionary conserved process that distinguishes intact chromo-

somes from chromosome fragments or other acentric DNA such as DNA viruses to facilitate removal of the latter from the nucleus.

S-Phase Micronucleation Suggests That Loss of p53 Function Affects the Probability of Chromosome Breakage

Treatment of normal fibroblasts with HU or PALA did not induce S-phase micronucleation, whereas identical treatment of isogenic p53-deficient normal fibroblasts increased S-phase micronucleation frequency significantly. These data, along with previous observations, lead us to propose that this micronucleation increase most likely reflects a higher probability of DNA breakage occurring in the p53-deficient cells when they attempt DNA replication under adverse conditions. In support of this idea, micronucleation is an indicator of chromosome breakage, and has long been used as an assay for clastogens (Heddle et al., 1991). Inhibition of replication fork progression induces chromosome breakage in bacteria, yeast, and mammals (Eki et al., 1987; Kuzminov, 1995; Michel et al., 1997). Furthermore, replication inhibitors including PALA, methotrexate, and aphidicolin can induce chromosome breakage through expression of fragile sites (Kuo et al., 1994; Coquelle et al., 1997). Although the relationship between fragile site induction and p53 function has not been tested, the cell lines used for such studies were competent for gene amplification and consequently should have had a defective p53 pathway (Livingstone et al., 1992; Yin et al., 1992). Consistent with a breakage-moderating function of p53, we previously reported that PALA generates chromosome damage in cells with defective, but not normal, p53 function (Linke et al., 1996). Taken together, the data lead us to propose that p53 minimizes the frequency at which structural chromosomal alterations are induced during exposure to suboptimal growth conditions by at least two mechanisms. First, as shown previously, p53 mediates a G1 arrest in response to low rNTP pools, which prevents cells from entering S phase with inadequate precursors for DNA replication (Linke et al., 1996). Second, the data presented here suggest that p53 minimizes S-phase DNA breakage in cells that attempt DNA replication during diverse metabolic challenges. The mechanisms underlying the proposed S-phase function of p53 are currently under investigation.

Micronucleation and Cancer Treatment

Drugs that enhance S-phase budding should prove valuable for chemotherapy as they affect a process (micronucleation) and cytogenetic aberration (DMs) that are restricted to cancer cells. However, their efficacy is limited by the extent to which DM removal prevents further cell growth, or enhances sensitivity to other therapeutic strategies. In COLO 320DM cells, induction of the S-phase budding mechanism can decrease the number of DMs sufficiently to reduce plating efficiency in soft agar and tumorigenicity *in vivo* (Von Hoff et al., 1992). Interestingly, COLO 320HSR cells, which have approximately the same number of *c-myc* genes amplified within chromosomes, did not exhibit such phenotypic changes upon HU treatment and did not decrease *c-myc* copy number, even though they produced ap-

proximately the same number of micronuclei as COLO 320DM cells (Von Hoff et al., 1992). The same HU treatment conditions also induced apoptosis more rapidly and in a higher fraction of COLO 320DM than COLO 320HSR cells (data not shown). Similarly, HU treatment of HL-60 DM, but not HL-60 HSR cells, reduced *c-myc* copy number, induced differentiation, and later, apoptosis (Eckhardt et al., 1994; Shimizu et al., 1994). These results suggest that reduced tumorigenicity may result from induction of an apoptotic program when a sufficient number of extrachromosomally amplified sequences encoding oncogenes are removed from the cell. The recognition of a mechanism for the segregation and elimination of amplified sequences and other acentric DNA macromolecules, and the recognition that some agents can enhance this process, present important opportunities to expand and refine chemotherapeutic strategies, and to gain insight into the *cis*-acting elements and *trans*-acting factors that determine nuclear DNA localization.

We would like to acknowledge S.P. Linke (National Cancer Institute, Bethesda, MD) for kindly providing cell lines. D. Peterson (Salk Institute, La Jolla, CA) for his kind help on the operation of confocal microscopy that appeared in Fig. 6, and D. Von Hoff and K. Davidson (both from Institute of Drug Development, University of Texas Health Science Center, San Antonio, TX) for allowing us to cite their unpublished results. We thank T. Shimura and N. Kumon (both from Hiroshima University, Higashi-Hiroshima, Japan) for their technical help. T. Paulson, T. Kanda, S. O'Gorman, S. Pfaff, G. Karpen, O. Vafa, and L.-c. Huang (all from Salk Institute except Paulson [Fred Hutchinson Cancer Research Center, Seattle, WA] and Huang [UBI, Menlo Park, CA]) provided helpful discussions concerning experimental procedures and topics presented in this manuscript.

This work was in part supported by a grant from the United States Department of Army, (grant number DAMD17-94-J4359) and the International Collaboration Grant from Japanese Ministry of Education (grant number 07044271), and the G. Harold and Leila Y. Mathers Charitable Foundation.

Received for publication 7 October 1997 and in revised form 16 December 1997.

References

- Alitalo, K., and M. Shwab. 1986. Oncogene amplification in tumor cells. *Adv. Cancer Res.* 47:235-281.
- Barker, P.E. 1982. Double minutes in human tumor cells. *Cancer Genet. Cytogenet.* 5:81-94.
- Benner, S.E., G.M. Wahl, and D.D. Von Hoff. 1991. Double minute chromosomes and homogeneously staining regions in tumors taken directly from patients versus in human tumor cell lines. *Anti-Cancer Drugs.* 2:11-25.
- Bondy, M.L., M.R. Spitz, S. Halabi, J.J. Fueter, S.P. Schantz, D. Sample, and T.C. Hsu. 1993. Association between family history of cancer and mutagen sensitivity in upper aerodigestive tract cancer patients. *Cancer Epidemiol. Biomarkers Prev.* 2:103-106.
- Brisson, O. 1993. Gene amplification and tumor progression. *Biochim. Biophys. Acta.* 1155:25-41.
- Canute, G.W., S.L. Longo, J.A. Longo, J.A. Winfield, B.H. Nevaldine, and P.J. Hahn. 1996. Hydroxyurea accelerates the loss of epidermal growth factor receptor genes amplified as double-minute chromosomes in human glioblastoma multiforme. *Neurosurgery.* 39:976-983.
- Carroll, S.M., J. Trotter, and G.M. Wahl. 1991. Replication timing control can be maintained in extrachromosomally amplified genes. *Mol. Cell Biol.* 11: 4779-4785.
- Carroll, S.M., M.L. DeRose, J.L. Kolman, G.H. Nonet, R.E. Kelly, and G.M. Wahl. 1993. Localization of a bidirectional DNA replication origin in the native locus and in episomally amplified murine adenosine deaminase loci. *Mol. Cell Biol.* 13:2971-2981.
- Cassimeris, L., and E.D. Salmon. 1991. Kinetochore microtubules shorten by loss of subunits at the kinetochores of prometaphase chromosomes. *J. Cell Sci.* 151-158.
- Cohen, S. 1993. Apoptosis. *Immunol. Today.* 14:126-130.
- Coquelle, A., E. Pipiras, F. Toledo, G. Buttin, and M. Debatisse. 1997. Expression of fragile sites triggers intrachromosomal mammalian gene amplification and sets boundaries to early amplicons. *Cell.* 89:215-225.
- Cowell, J.K. 1982. Double minutes and homogeneously staining regions: gene amplification in mammalian cells. *Annu. Rev. Gen.* 16:21-59.
- Cremer, T., A. Kurz, R. Zirbel, S. Dietzel, B. Rinke, E. Schrock, M.R. Speicher, U. Mathieu, A. Jauch, and P. Emmerich. 1993. Role of chromosome territories in the functional compartmentalization of the cell nucleus. *Cold Spring Harbor Symp. Quant. Biol.* 58:777-792.
- Crook, T., J.A. Tidy, and K.H. Vousden. 1991. Degradation of p53 can be targeted by HPV E6 sequences distinct from those required for p53 binding and trans-activation. *Cell.* 67:547-556.
- DeBoni, U., and A.H. Mintz. 1986. Curvilinear, three-dimensional motion of chromatin domains and nucleoli in neuronal interphase nuclei. *Science.* 234: 863-866.
- Denko, N.C., A.J. Giaccia, J.R. Stringer, and P.J. Stambrook. 1994. The human Ha-ras oncogene induces genomic instability in murine fibroblasts within one cell cycle. *Proc. Natl. Acad. Sci. USA.* 91:5124-5128.
- Di Leonardo, A., S.P. Linke, K. Clarkin, and G.M. Wahl. 1994. DNA damage triggers a prolonged p53-dependent G1 arrest and long-term induction of Cip1 in normal human fibroblasts. *Genes Dev.* 8:2540-2551.
- Dini, L., S. Coppola, M.T. Ruzittu, and L. Ghibelli. 1996. Multiple pathways for apoptotic nuclear fragmentation. *Exp. Cell Res.* 223:340-347.
- Duncan, A.M., and J.A. Heddle. 1984. The frequency and distribution of apoptosis induced by three non-carcinogenic agents in mouse colonic crypts. *Cancer Lett.* 23:307-311.
- Duncan, A.M., J.A. Heddle, and D.H. Blakey. 1985. Mechanism of induction of nuclear anomalies by gamma-radiation in the colonic epithelium of the mouse. *Cancer Res.* 45:250-252.
- Dyer, K.A., T.K. Canfield, and S.M. Gartler. 1989. Molecular cytological differentiation of active from inactive X domains in interphase: implications for X chromosome inactivation. *Cytogenet. Cell Genet.* 50:116-120.
- Eckhardt, S.G., A. Dai, K.K. Davidson, B.J. Forseth, G.M. Wahl, and D.D. Von Hoff. 1994. Induction of differentiation in HL60 cells by the reduction of extrachromosomally amplified *c-myc*. *Proc. Natl. Acad. Sci. USA.* 91: 6674-6678.
- Eki, T., T. Enomoto, Y. Murakami, F. Hanaoka, and M. Yamada. 1987. Characterization of chromosome aberrations induced by incubation at a restrictive temperature in the mouse temperature-sensitive mutant tsFT20 strain containing heat-labile DNA polymerase α . *Cancer Res.* 47:5162-5170.
- Ferguson, M., and D.C. Ward. 1992. Cell cycle dependent chromosomal movement in pre-mitotic human T-lymphocyte nuclei. *Chromosoma.* 101:557-565.
- Gaubatz, J.W. 1990. Extrachromosomal circular DNA and genomic sequence plasticity in eukaryotic cells. *Mutat. Res.* 237:271-292.
- Gavrieli, Y., Y. Sherman, and S.S. Ben. 1992. Identification of programmed cell death in situ via specific labeling of nuclear DNA fragmentation. *J. Cell Biol.* 119:493-501.
- Hamkalo, B.A., P.J. Farnham, R. Johnston, and R.T. Schimke. 1985. Ultrastructural features of min chromosomes in a methotrexate-resistant mouse 3T3 cell line. *Proc. Natl. Acad. Sci. USA.* 82:1026-1030.
- Hartwell, L.H., and M.B. Kastan. 1994. Cell cycle control and cancer. *Science.* 266:1821-1828.
- Heddle, J.A., and A.V. Carrano. 1977. The DNA content of micronuclei induced in mouse bone marrow by γ -irradiation: evidence that micronuclei arise from acentric chromosomal fragments. *Mutat. Res.* 44:63-69.
- Heddle, J.A., M.C. Cimino, M. Hayashi, F. Romagna, M.D. Shelby, J.D. Tucker, P. Vanparys, and J.T. MacGregor. 1991. Micronuclei as an index of cytogenetic damage: past, present, and future. *Environ. Mol. Mutagen.* 18: 277-291.
- Heddle, J.A., M. Hite, B. Kirkhart, K. Mavournin, J.T. MacGregor, G.W. Newell, and M.F. Salamone. 1983. The induction of micronuclei as a measure of genotoxicity. A report of the U.S. Environmental Protection Agency Genotox Program. *Mutat. Res.* 123:61-118.
- Huang, L.-c., K.C. Clarkin, and G.M. Wahl. 1996. p53 dependent cell cycle arrests are preserved in DNA-activated protein kinase deficient mouse fibroblasts. *Cancer Res.* 56:2940-2944.
- Jackson, J.F., and E.G. Clement. 1974. Letter: nuclear projections and chromosome abnormalities. *Lancet.* 2:1270-1271.
- Kastan, M.B., Q. Zhan, W.S. El-Deiry, F. Carrier, T. Jacks, W.V. Walsh, B.S. Plunkett, B. Vogelstein, and A.J. Fornace. 1992. A mammalian cell cycle checkpoint pathway utilizing p53 and GADD45 is defective in ataxia-telangiectasia. *Cell.* 71:587-597.
- Kuerbitz, S.J., B.S. Plunkett, W.V. Walsh, and M.B. Kastan. 1992. Wild-type p53 is a cell cycle checkpoint determinant following irradiation. *Proc. Natl. Acad. Sci. USA.* 89:7491-7495.
- Kuo, M.T., R.C. Vyas, L.X. Jiang, and W.N. Hittelman. 1994. Chromosome breakage at a major fragile site associated with P-glycoprotein gene amplification in multidrug-resistant CHO cells. *Mol. Cell Biol.* 14:5202-5211.
- Kuzminov, A. 1995. Instability of inhibited replication forks in *E. coli*. *Bioessays.* 17:733-741.
- Lawce, H.J., and G. Brown. 1991. Harvesting, Slide Making, and Chromosome Elongation Techniques. M.J. Barch, editor. Raven Press, Ltd. New York. 31-66.
- Levan, A., and G. Levan. 1978. Have double minutes functioning centromeres? *Hereditas.* 88:81-92.
- Levan, G., N. Mandahl, U. Bregula, G. Klein, and A. Levan. 1976. Double minute chromosomes are not centromeric regions of the host chromosomes.

- Hereditas*. 83:83-90.
- Linke, S.P., K.C. Clarkin, A. Di Leonardo, A. Tsou, and G.M. Wahl. 1996. A reversible p53-dependent G0/G1 cell cycle arrest induced by ribonucleotide depletion in the absence of detectable DNA damage. *Genes Dev.* 10:934-947.
- Linke, S.P., K.C. Clarkin, and G.M. Wahl. 1997. p53 mediates permanent arrest over multiple cell cycles in response to gamma irradiation. *Cancer Res.* 57: 1171-1179.
- Livingstone, L.R., A. White, J. Sprouse, E. Livanos, T. Jacks, and T.D. Tlsty. 1992. Altered cell cycle arrest and gene amplification potential accompany loss of wild-type p53. *Cell*. 70:923-935.
- Lo, C.F., and M. Fraccaro. 1974. Letter: nuclear projections in tumour cells. *Lancet*. 2:847.
- Madireddi, M.T., R.S. Coyne, J.F. Smothers, K.M. Mickey, M.C. Yao, and C.D. Allis. 1996. Pdd1p, a novel chromodomain-containing protein, links heterochromatin assembly and DNA elimination in *Tetrahymena*. *Cell*. 87:75-84.
- Manuelidis, L., and J. Borden. 1988. Reproducible compartmentalization of individual chromosome domains in human CNS cells revealed by in situ hybridization and three-dimensional reconstruction. *Chromosoma (Berl.)*. 96: 397-410.
- Michel, B., S.D. Ehrlich, and M. Uzest. 1997. DNA double-strand breaks caused by replication arrest. *EMBO (Eur. Mol. Biol. Organ.) J.* 16:430-438.
- Miele, M., S. Bonatti, P. Menichini, L. Ottaggio, and A. Abbondandolo. 1989. The presence of amplified regions affects the stability of chromosomes in drug-resistant Chinese hamster cells. *Mutat. Res.* 219:171-178.
- O'Keefe, R.T., S.C. Henderson, and D.L. Spector. 1992. Dynamic organization of DNA replication in mammalian cell nuclei: Spatially and temporally defined replication of chromosome-specific α -satellite DNA sequences. *J. Cell Biol.* 116:1095-1110.
- Pedeutour, F., R.F. Suijkerbuijk, A. Forus, G.J. Van de Klundert, W.J.M. Coindre, G. Nicolo, F. Collin, U. VanHaelst, K. Huffermann et al. 1994. Complex composition and co-amplification of SAS and MDM2 in ring and giant rod marker chromosomes in well-differentiated liposarcoma. *Genes Chromosom. Cancer*. 10:85-94.
- Roser, M., A. Bohm, M. Oldigs, M. Weichenthal, U. Reimers, P.U. Schmidt, E.W. Breitbart, and H.W. Rudiger. 1989. Ultraviolet-induced formation of micronuclei and sister chromatid exchange in cultured fibroblasts of patients with cutaneous malignant melanoma. *Cancer Genet. Cytogenet.* 41:129-137.
- Ruddle, F.H. 1962. Nuclear bleb: a stable interphase marker in established line of cells in vitro. *J. Natl. Cancer Inst.* 28:1247-1251.
- Satoh, M.S., and T. Lindahl. 1992. Role of poly (ADP-ribose) formation in DNA repair. *Nature*. 356:356-358.
- Scheffner, M., B.A. Werness, J.M. Huibregtse, A.J. Levine, and P.M. Howley. 1990. The E6 oncoprotein encoded by human papillomavirus types 16 and 18 promotes the degradation of p53. *Cell*. 63:1129-1136.
- Schubert, I., and J.L. Oud. 1997. There is an upper limit of chromosome size for normal development of an organism. *Cell*. 88:515-520.
- Shima, H., M. Nakayasu, S. Aonuma, T. Sugimura, and M. Nagao. 1989. Loss of the MYC gene amplified in human HL-60 cells after treatment with inhibitors of poly (ADP-ribose) polymerase or with dimethyl sulfoxide. *Proc. Natl. Acad. Sci. USA*. 86:7442-7445.
- Shimizu, N., T. Kanda, and G.M. Wahl. 1996. Selective capture of acentric fragments by micronuclei provides a rapid method for purifying extrachromosomally amplified DNA. *Nat. Genet.* 12:65-71.
- Shimizu, N., H. Nakamura, T. Kadota, K. Kitajima, T. Oda, T. Hirano, and H. Utiyama. 1994. Loss of amplified c-myc genes in the spontaneously differentiated HL-60 cells. *Cancer Res.* 54:3561-3567.
- Snapka, R.M. 1992. Gene amplification as a target for cancer chemotherapy. *Oncol. Res.* 4:145-150.
- Snapka, R.M., and A. Varshavsky. 1983. Loss of unstably amplified dihydrofolate reductase genes from mouse cells is greatly accelerated by hydroxyurea. *Proc. Natl. Acad. Sci. USA*. 80:7533-7537.
- Stein, S.J., J.L. Stein, J.B. Lian, T.J. Last, T. Owen, and L. McCabe. 1994. Synchronization of Normal Diploid and Transformed Mammalian Cells. J.E. Celis, editor. Academic Press, San Diego, CA. 282-287.
- Toledo, F., R.D. Le, G. Buttin, and M. Debatisse. 1992. Co-amplified markers alternate in megabase long chromosomal inverted repeats and cluster independently in interphase nuclei at early steps of mammalian gene amplification. *EMBO (Eur. Mol. Biol. Organ.) J.* 11:2665-2673.
- Tucker, J.D., J. Nath, and J.C. Hando. 1996. Activation status of the X-chromosome in human micronucleated lymphocytes. *Human Genet.* 97:471-475.
- Von Hoff, D., D. Needham-VanDevanter, J. Yucel, B. Windle, and G. Wahl. 1988. Amplified human MYC oncogenes localized to replicating submicroscopic circular DNA molecules. *Proc. Natl. Acad. Sci. USA*. 85:4804-4808.
- Von Hoff, D.D., J.R. McGill, B.J. Forseth, K.K. Davidson, T.P. Bradley, D.R. Van Devanter, and G.M. Wahl. 1992. Elimination of extrachromosomally amplified MYC genes from human tumor cells reduces their tumorigenicity. *Proc. Natl. Acad. Sci. USA*. 89:8165-8169.
- Von Hoff, D.D., T. Waddelow, B. Forseth, K. Davidson, J. Scott, and G.M. Wahl. 1991. Hydroxyurea accelerates the loss of extrachromosomally amplified genes from tumor cells. *Cancer Res.* 51:6273-6279.
- Vouret, C., D. Taruscio, A.L. Boyle, and D.C. Ward. 1993. Cell cycle-dependent distribution of telomeres, centromeres, and chromosome-specific sub-satellite domains in the interphase nucleus of mouse lymphocytes. *Exp. Cell Res.* 205:142-151.
- Wahl, G.M. 1989. The importance of circular DNA in mammalian gene amplification. *Cancer Res.* 49:1333-1340.
- White, A.E., E.M. Livanos, and T.D. Tlsty. 1994. Differential disruption of genomic integrity and cell cycle regulation in normal human fibroblasts by the HPV oncoproteins. *Genes Dev.* 8:666-677.
- White, E. 1994. Tumour biology. p53, guardian of Rb. *Nature*. 371:21-22.
- Yin, Y., M.A. Tainsky, F.Z. Bischoff, L.C. Strong, and G.M. Wahl. 1992. Wild-type p53 restores cell cycle control and inhibits gene amplification in cells with mutant p53 alleles. *Cell*. 70:937-948.

Histone-GFP fusion protein enables sensitive analysis of chromosome dynamics in living mammalian cells

Teru Kanda*, Kevin F. Sullivan† and Geoffrey M. Wahl*

Background: The amplification of oncogenes in cancer cells is often mediated by paired acentric chromatin bodies called double minute chromosomes (DMs), which can accumulate to a high copy number because of their autonomous replication during the DNA synthesis phase of the cell cycle and their subsequent uneven distribution to daughter cells during mitosis. The mechanisms that control DM segregation have been difficult to investigate, however, as the direct visualization of DMs in living cells has been precluded because they are far smaller than normal chromosomes. We have visualized DMs by developing a highly sensitive method for observing chromosome dynamics in living cells.

Results: The human histone H2B gene was fused to the gene encoding the green fluorescent protein (GFP) of *Aequorea victoria* and transfected into human HeLa cells to generate a stable line constitutively expressing H2B-GFP. The H2B-GFP fusion protein was incorporated into nucleosomes without affecting cell cycle progression. Using confocal microscopy, H2B-GFP allowed high-resolution imaging of both mitotic chromosomes and interphase chromatin, and the latter revealed various chromatin condensation states in live cells. Using H2B-GFP, we could directly observe DMs in living cancer cells; DMs often clustered during anaphase, and could form chromosomal 'bridges' between segregating daughter chromosomes. Cytokinesis severed DM bridges, resulting in the uneven distribution of DMs to daughter cells.

Conclusions: The H2B-GFP system allows the high-resolution imaging of chromosomes, including DMs, without compromising nuclear and chromosomal structures and has revealed the distinctive clustering behavior of DMs in mitotic cells which contributes to their asymmetric distribution to daughter cells.

Background

In eukaryotes, segregation of sister chromatids during mitosis requires spindle fiber attachment to the kinetochores formed at centromeric DNA. Cancer cells often harbor abnormal chromosomes such as dicentric or acentric chromosomes, however, which would be expected to behave anomalously. Double minute chromosomes (DMs) are paired chromatin bodies that have been reported in as many as 50% of human tumors but have never been observed in normal cells [1,2]. As DMs lack functional centromeres, they do not segregate by the same mechanism used by normal chromosomes. DMs can accumulate to a high copy number because of their autonomous replication during the DNA synthesis (S) phase of the cell cycle and their subsequent uneven distribution to daughter cells during mitosis. As DMs contain a diversity of amplified oncogenes [3], their uneven segregation and accumulation increases the malignant potential during tumor progression. On the other hand, as DM loss can decrease tumor cell viability [4], understanding the mechanism of DM segregation could lead to the identification

of highly selective anti-neoplastic agents that specifically disrupt the transmission of DMs to daughter cells.

Observations of fixed chromosomes in DM-harboring cancer cells have provided some insights into DM segregation during mitosis [5,6]. Fixation and permeabilization of cells may cause artificial distortions of chromosome distribution, however, and could perturb intracellular structures. An ideal strategy for examining the dynamics of DM segregation would involve their direct visualization in living cells. DMs vary in size, however, and many are at the size limit of conventional cytogenetics ($\sim 1\text{--}2 \times 10^6$ bp) [2], which has prevented their detection in cycling cells. This report describes a fluorescent labeling system with sufficient sensitivity to visualize DMs *in vivo*, and that enables analyses of their segregation dynamics in real time during mitosis.

One approach to label chromosomes in living cells involves the fluorescent tagging of proteins that localize to chromosomes. The nucleosome is the fundamental repeating unit

Addresses: *Gene Expression Laboratory, The Salk Institute for Biological Studies, 10010 N. Torrey Pines Road, La Jolla, California 92037, USA.

†Department of Cell Biology, The Scripps Research Institute, La Jolla, California 92037, USA.

Correspondence: Geoffrey M. Wahl
E-mail: wahl@salk.edu

Received: 17 December 1997

Revised: 12 February 1998

Accepted: 18 February 1998

Published: 10 March 1998

Current Biology 1998, 8:377–385

<http://biomednet.com/elecref/0960982200800377>

© Current Biology Ltd ISSN 0960-9822

of chromatin. Each nucleosome core particle consists of an octamer of core histones with 146 bp of micrococcal-nuclease-resistant DNA wrapped around it [7]. As histones are the principal structural proteins of eukaryotic chromosomes, they are attractive targets for fluorescent labeling. Purified calf thymus histones (H2A and H2B) conjugated with rhodamine have been microinjected into *Drosophila* embryos to analyze cell lineage relationships [8] and chromosomal condensation and decondensation events [9]. The success of this approach demonstrates the utility of fluorescently labeled histones to study chromosomal dynamics in living cells.

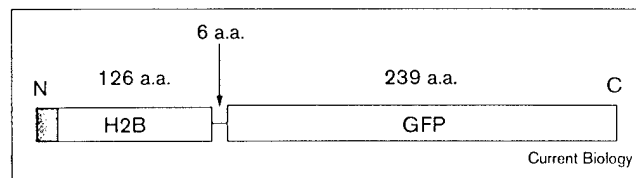
The green fluorescent protein (GFP) of the jellyfish *Aequorea victoria* retains its fluorescent properties when recombinant GFP proteins are expressed in eukaryotic cells [10]. GFP fusion proteins have been successfully targeted to specific subcellular organelles and structures including the nucleus, plasma membrane, mitochondrion, cytoskeleton, and Golgi apparatus [11–13]. Recently, GFP tagging also enabled visualization of specific chromosomal regions [14–16]. These results indicate the potential utility of a histone–GFP fusion protein to fluorescently label chromosomes in living cells. The feasibility of this approach is indicated by the observation that a fusion protein of GFP and yeast histone H2B localized properly in yeast nuclei [17]. Here, we show that a fusion protein of GFP and human H2B (H2B–GFP) is incorporated into nucleosome core particles without perturbing cell cycle progression. H2B–GFP bound chromosomes and DMs with high specificity, allowing them to be easily observed using a confocal microscope. We describe for the first time the behavior of DMs during mitosis in living cells. Our results reveal that DMs often cluster in anaphase cells and attach to groups of segregating chromosomes. Sometimes, segregating daughter chromosomes are connected by DM ‘bridges’ spanning the midplane of anaphase cells. Time-lapse observation revealed that cytokinesis severs the DM bridges, resulting in asymmetric distribution of DMs to the daughter cells.

Results

Stable expression of H2B–GFP in HeLa cells

The cDNA encoding human H2B was tagged at its carboxyl terminus with DNA encoding codon-optimized enhanced GFP [18] (Figure 1), and the chimeric gene was subcloned into a mammalian expression vector. The construct was introduced into the human HeLa cell line by transient transfection, and fluorescence microscopic observation indicated that H2B–GFP protein localized to interphase nuclei and mitotic chromosomes (data not shown). To analyze the effects of constitutively H2B–GFP expression on cell cycle progression, we transfected HeLa cells and cultured them under drug selection (blasticidin) to obtain clones that stably expressed the H2B–GFP transgene. GFP-positive colonies arose in about 10% of

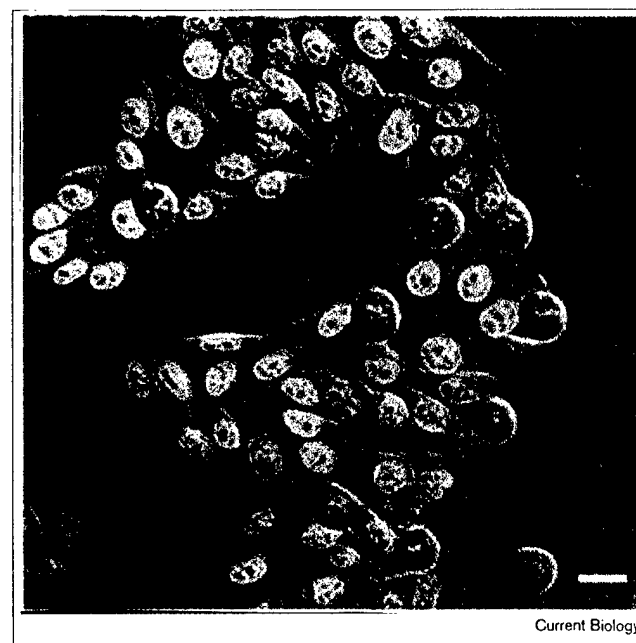
Figure 1



The H2B–GFP chimeric protein. The H2B protein was tagged with GFP at its carboxyl terminus; the length, in amino acids (a.a.), of each region and of the junction between H2B and GFP is indicated. The amino (N) and carboxyl (C) termini of the fusion protein are indicated and the histone amino-terminal tail is shown as a gray box.

blasticidin-resistant colonies, while other colonies (~90%) were negative for GFP for unknown reasons. We obtained several stable cell lines expressing H2B–GFP. A cell line with uniform, high-level expression of H2B–GFP was chosen for further analyses (Figure 2). The expression level of H2B–GFP in this cell line was stable for more than three months in the absence of continuous blasticidin selection. The high degree of stability of the integrated H2B–GFP gene in the absence of selection strongly suggests that chromosome stability is unimpaired by constitutive H2B–GFP expression. The mitotic index and the growth rate of this cell line were similar to those of the

Figure 2



Cells expressing H2B–GFP. A confocal microscopic image of live HeLa cells constitutively expressing H2B–GFP; the GFP fluorescence (green) was overlaid onto a differential interference contrast image. The figure shows that H2B–GFP is detected highly efficiently in cells in all phases of the cell cycle and that H2B–GFP is contained solely in the nucleus. The scale bar is 25 μ m.

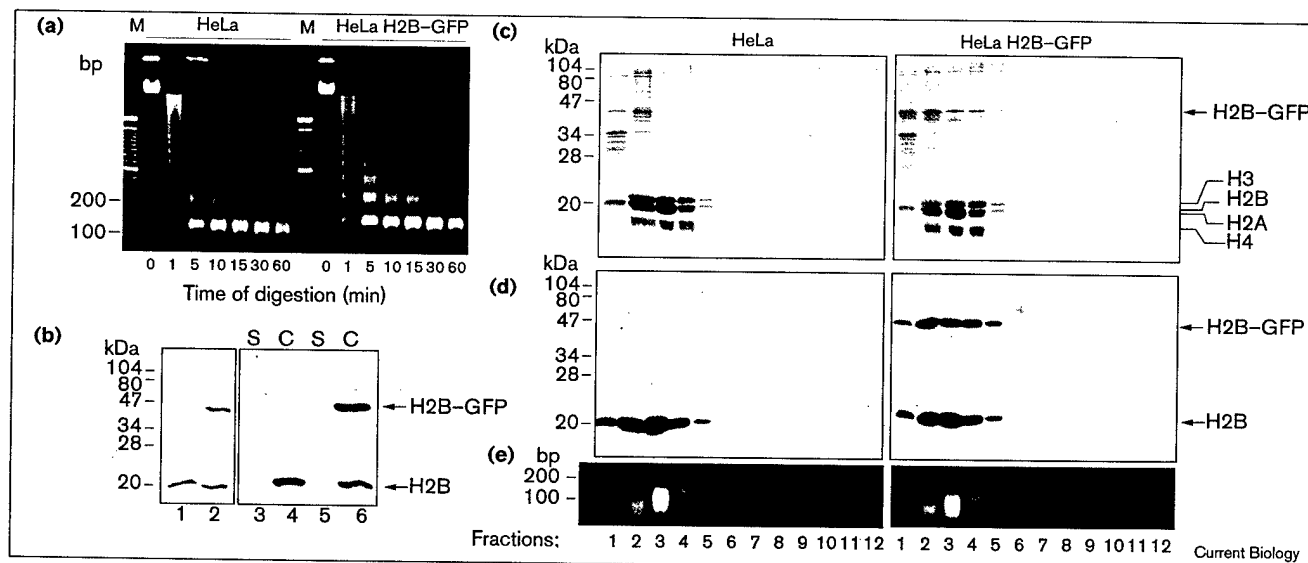
parental HeLa cells (data not shown). We also used a cell line stably expressing a fusion protein of H2B fused at its amino terminus to GFP and got essentially the same results (data not shown).

H2B-GFP is incorporated into nucleosomes

We biochemically fractionated nucleosome core particles from cells expressing H2B-GFP and analyzed for the presence of the fusion protein to determine if it was a component of nucleosome core particles. Mononucleosomes were generated by extensive micrococcal nuclease digestion of the isolated nuclei expressing H2B-GFP (Figure 3a). Digested chromatin was pelleted by subsequent centrifugation of the nuclease-treated nuclei. The supernatant and pellet, together with whole cell lysate of HeLa cells and HeLa cells expressing H2B-GFP, were analyzed by western blotting using an anti-human-H2B antibody. The majority of the expressed H2B-GFP protein was recovered in the pelleted chromatin fraction, and little if any was detected in the supernatant (Figure 3b, compare lane 5 with lane 6). The chromatin fraction was further fractionated by sucrose gradient centrifugation in the presence of 0.5 M NaCl to dissociate

histone H1 [19]. Electrophoretic analysis of the DNA showed that fractions 2 through 4 (predominantly fraction 3) contained DNA of about 146 bp (the size expected for the DNA wrapped around nucleosome core particles; Figure 3e). The proteins in the samples were analyzed by gel electrophoresis; H2B-GFP protein and core histones were identified in the mononucleosome fractions by Coomassie staining (Figure 3c). Aliquots of the same samples were analyzed by western blotting using anti-human-H2B antibody to specifically detect H2B and H2B-GFP protein (Figure 3d). The results demonstrate that the H2B-GFP fusion protein is in the mononucleosome fractions of the sucrose gradient and that its distribution parallels that of native histones in the gradient. The relative amounts of H2B-GFP and endogenous H2B in the purified mononucleosomes (Figure 3d) were comparable to their relative amounts in the whole cell lysate (Figure 3b, lane 2), suggesting that H2B-GFP protein is incorporated into nucleosomes efficiently. H2B-GFP association with the nucleosome core particle was stable under conditions that dissociate histone H1 [19], suggesting that adventitious aggregation of H2B-GFP protein with chromatin is unlikely (see Discussion).

Figure 3



H2B-GFP is incorporated into mononucleosomes. (a) Micrococcal nuclease digestion of nuclei from HeLa cells and HeLa cells expressing H2B-GFP. Isolated nuclei were digested for 0, 1, 5, 10, 15, 30, and 60 min, as indicated, and the DNA protected from digestion by the binding of nucleosomal core proteins was analyzed by 1.5% agarose gel electrophoresis. The markers used (M) were 100 bp ladders. (b) Whole cell lysate (25 μ g each from HeLa cells, lane 1, or HeLa cells expressing H2B-GFP, lane 2), supernatants (S) and soluble chromatin fractions (C) of the digested nuclei (10 μ g each from HeLa cells, lanes 3 and 4, or HeLa cells expressing H2B-GFP, lanes 5 and 6) were analyzed by western blotting using anti-human-H2B antibody. Soluble chromatin fractions were prepared as described in Materials and methods. H2B-GFP protein (approximately

45 kDa) and endogenous H2B protein are indicated. (c) Sucrose gradient analysis of mononucleosome populations. The mononucleosome protein-DNA complexes from HeLa cells and HeLa cells expressing H2B-GFP, prepared by micrococcal nuclease digestion, were purified through parallel 5–30% sucrose gradients. Proteins from each fraction were extracted and analyzed by electrophoresis through SDS–15% polyacrylamide gels and Coomassie staining. H2B-GFP protein and the native core histone proteins (H2A, H2B, H3 and H4) are indicated. (d) Aliquots of the fractions in (c) were electrophoresed and analyzed by western blotting using anti-human-H2B antibody. H2B-GFP protein and endogenous H2B protein are indicated. (e) DNA in each fraction was analyzed by 1.5% agarose gel electrophoresis.

H2B-GFP incorporation does not inhibit cell cycle progression

It was conceivable that GFP tagging of H2B protein could affect chromatin structure and perturb cell cycle progression as a consequence. Therefore, the cell cycle distribution of the established cell line expressing H2B-GFP was analyzed to ascertain differences in cell cycle progression relative to the parental cell population. Asynchronous HeLa cells and the transformant expressing H2B-GFP were fixed with ethanol, stained with propidium iodide (PI), and analyzed by fluorescence-activated cell sorting (FACS). The green emission of GFP-labeled cells produced an approximately three-log shift from parental HeLa cells (Figure 4a,b). DNA content was determined by measuring the red emission of PI (Figure 4c,d). The results indicate that the cell cycle distribution of asynchronous HeLa cells expressing H2B-GFP is indistinguishable from that of the parental HeLa cells, clearly demonstrating that the H2B-GFP protein has little, if any, effect on cell cycle progression.

H2B-GFP decorates chromosomes in living cells

Cells expressing H2B-GFP were observed using confocal microscopy to determine the pattern of chromatin staining in interphase and mitosis. As shown in Figure 5, H2B-GFP enabled highly sensitive chromatin detection

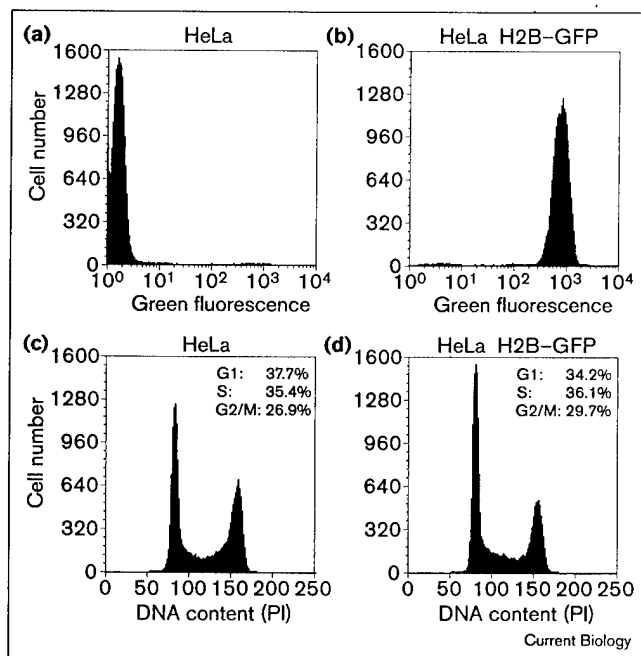
in all phases of the cell cycle. Fixation and permeabilization of the cells, which might cause artificial distortion of intracellular structure, was not required to obtain such images. H2B-GFP was highly specific for nuclear chromatin as no fluorescence was observed in the cytoplasm. In addition, H2B-GFP provided a remarkable level of sensitivity. For example, a chromatin structure that appeared to be a pair of lagging sister chromatids with a centromeric constriction was readily observed (Figure 5e). The fine intranuclear chromatin architecture in interphase nuclei visualized by H2B-GFP was consistent with the previously reported deconvoluted optical-sectioning images of fixed nuclei obtained by 4',6'-diamidino-2-phenylindole (DAPI) staining [20]. Chromosome spreads of the H2B-GFP-expressing cells also showed that the GFP fluorescence patterns were identical to the patterns obtained using DAPI (Figure 5i,j).

We also observed perinucleolar regions densely stained with H2B-GFP that resembled chromocenters in interphase nuclei (Figure 5a). A previously described feature of chromocenters is that they are heterochromatic and often contain centromeres [21,22]. Double staining with centromere antibodies and H2B-GFP demonstrated that certain regions with intense H2B-GFP staining possessed multiple centromeres (Figure 6). From this result, coupled with the concordance of H2B-GFP staining and DAPI staining (Figure 5i,j), we conclude that H2B-GFP staining reflects the density of packing of DNA in different regions of the nucleus. Thus, chromosomal domains that have previously only been examined in fixed cells may be monitored using the H2B-GFP method in living cells.

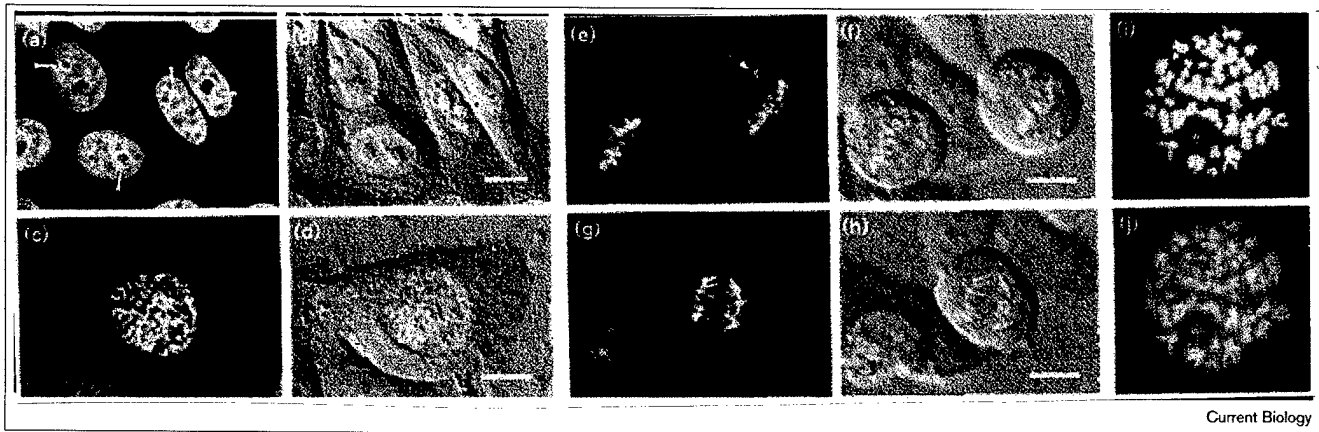
Visualization of DMs in living cells

We applied our highly sensitive H2B-GFP chromatin-labeling technique to the analysis of DMs in living cells. A retroviral vector was constructed to enable the efficient transfer and expression of H2B-GFP in a broad range of host cells. We used a vesicular stomatitis virus G glycoprotein (VSV-G) pseudotyped retroviral vector to obtain high viral titers [23]. COLO320DM cells harboring DMs containing an amplified *c-myc* gene [24,25] were infected with the H2B-GFP retrovirus, and two days later over 90% of the cells expressed H2B-GFP protein. FACS analyses revealed that cell cycle progression of COLO320DM cells was not affected by H2B-GFP expression (data not shown). We collected serial-sectioning images of living COLO320DM cells expressing H2B-GFP using confocal microscopy. We noticed that small fluorescent dots were frequently observed in mitotic cells (Figure 7a,b). The sizes of these dots were 0.7–0.85 μm in diameter, corresponding to the size of DMs in this cell line. We found that they frequently associated in clusters in anaphase cells where they were attached to normal chromosomes (Figure 7a). Sometimes they aligned in regular arrays and

Figure 4



H2B-GFP expression does not affect cell cycle progression. (a,c) HeLa cells and (b,d) HeLa cells expressing H2B-GFP were fixed with ethanol, stained with PI, and analyzed by FACS. (a,b) Flow cytometry histograms of GFP fluorescence. (c,d) Flow cytometry histograms of the DNA content determined by PI staining. The estimated proportion of cells in the G1, S, and G2/M fractions are indicated.

Figure 5

Localization of H2B-GFP protein. (a–h) Confocal microscopic images of live HeLa cells expressing H2B-GFP in various cell cycle phases. (a, c, e, g) The GFP fluorescence and (b, d, f, h) the corresponding differential interference contrast images are shown for (a, b) interphase, (c, d) prophase, (e, f) metaphase and (g, h) anaphase cells. Perinucleolar

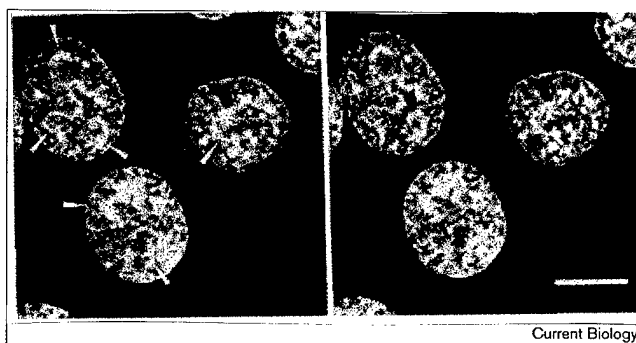
densely staining regions of H2B-GFP are indicated by arrowheads in (a). A pair of lagging sister chromatids with a centromeric constriction is indicated by an arrow in (e). The scale bars are 10 μ m. (i) GFP localization and (j) DAPI staining of fixed chromosome spreads of HeLa cells expressing H2B-GFP.

formed an extended bridge between segregating groups of daughter chromosomes (Figure 7b).

In order to confirm that these dot-like chromatin bodies were DMs, mitotic COLO320DM cells were fixed with or without colcemid treatment, and the DM distribution was analyzed by fluorescence *in situ* hybridization (FISH) using a *c-myc* cosmid probe. Whereas chromosome spreads of colcemid-treated cells usually had dispersed DMs (Figure 7c), DMs were observed to form clusters in untreated mitotic cells (Figure 7d,e). The DMs detected using FISH were strikingly similar to the dot-like structures observed in H2B-GFP-expressing cells (compare

Figure 7a,b to Figure 7d,e). The results strongly suggest that the dot-like chromatin bodies observed in living cells are DMs. We found that most of the observed mitotic cells contained clustered DMs, although the number of DMs varied from cell to cell. Approximately 30% of the anaphase cells showed bridge formations involving DMs. We therefore conclude that the clustering of DMs and their unbalanced distribution to daughter cells during mitosis are very common events in this cell line.

We next analyzed DM segregation by making time-lapse observations using an epifluorescence microscope (Figure 8). Clustered DMs were attached by the extended arms of normal segregating chromosomes, forming a chromosome bridge (Figure 8a). This bridge was further extended as daughter chromosomes segregated (Figure 8b). Subsequently, the bridge was severed by the process of cytokinesis (Figure 8c), and the cluster of DMs appeared to be unevenly distributed to daughter nuclei (Figure 8d). These results clearly demonstrate that DMs frequently cluster in anaphase cells, sometimes forming chromosomal bridges, and that their uneven distribution to daughter cells can result from cytokinesis severing DM bridges asymmetrically.

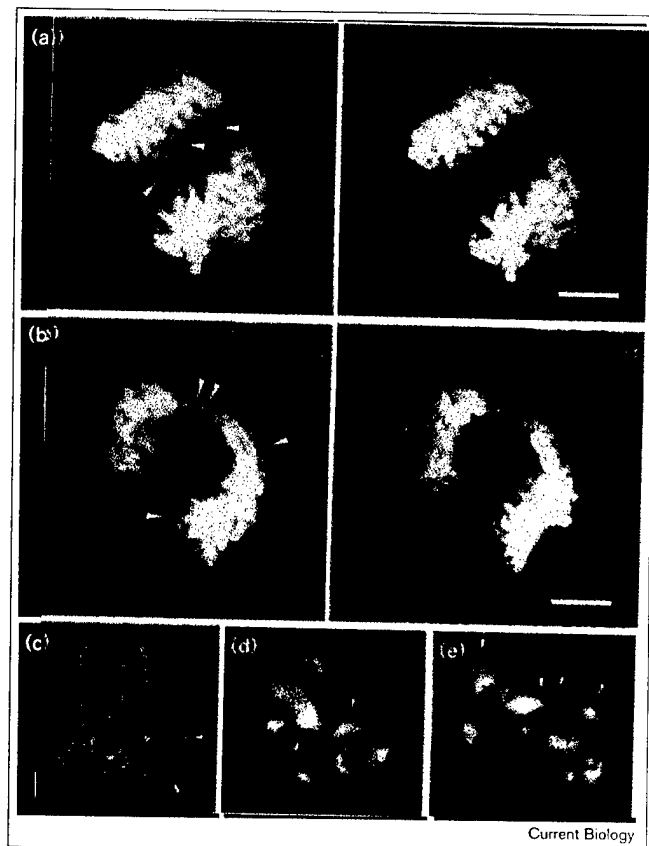
Figure 6

Perinucleolar regions densely stained with H2B-GFP possess multiple centromeres. Stereoscopic images of centromere localization in H2B-GFP-expressing HeLa cells. Centromeres were detected by immunofluorescence using a human anti-centromere antiserum. Localization of centromeres (red) and H2B-GFP (green) are indicated. Perinucleolar heterochromatic domains are indicated by arrowheads. The scale bar is 10 μ m.

Discussion

We have described a novel strategy to fluorescently label chromosomes in living cells and the successful application of this strategy to observe DMs in living cells. Despite the large size of the GFP tag (239 amino acids), it has been shown in numerous cases that GFP-tagged proteins are functional and localize properly [11–13]. Such is also the case with the histone H2B-GFP fusion protein. Our experimental data demonstrate the co-fractionation of

Figure 7

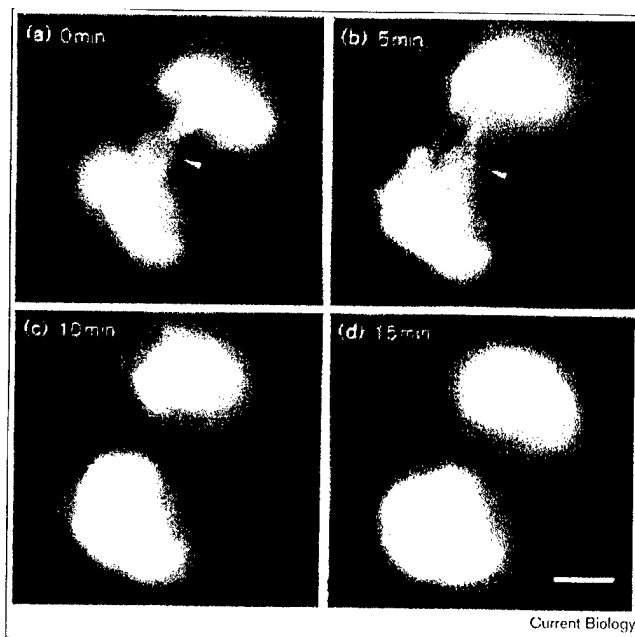


DMs cluster in anaphase cells. (a,b) Stereoscopic images of live COLO320DM cells expressing H2B-GFP. Clustered dot-like chromatin bodies (shown by arrowheads) together with segregating daughter chromosomes were visualized by GFP fluorescence (green). The scale bars are 5 μ m. (c) DMs were detected in a metaphase spread of colcemid-treated COLO320DM cells by fluorescence *in situ* hybridization (FISH) using a biotinylated *c-myc* cosmid probe and fluorescein-isothiocyanate-avidin. Chromosomes were counterstained with PI. (d,e) Asynchronously growing COLO320DM cells were directly fixed on chamber slides without colcemid treatment and processed for FISH analyses with the *c-myc* cosmid probe. Clustered DMs (arrowheads) and segregating daughter chromosomes (PI stained; red) are shown. Fluorescence images were collected using an epifluorescence microscope.

H2B-GFP with mononucleosomes under high ionic strength (0.5 M NaCl). The primary interactions responsible for the stability of nucleosomes are electrostatic as nucleosomes can be dissociated into their DNA and histone components by elevating ionic strength. Histone H1, as well as non-histone proteins, dissociates from the nucleosomes at 0.5 M NaCl [7,19]. It is therefore likely that H2B-GFP protein is incorporated into nucleosome core particles rather than just affiliating with the core particles by a non-specific electrostatic interaction.

The strategy described in this paper offers significant advantages over other chromosome-labeling methods. Although fluorescent labeling of mammalian chromosomes

Figure 8



Transmission of DMs to daughter cells visualized in living cells. Time-lapse imaging of an H2B-GFP-labeled COLO320DM cell from late anaphase to telophase. A cluster of lagging DMs (shown by arrowheads) formed a bridge between segregating chromosomes, and the bridge was severed by cytokinesis. Fluorescence images were collected at the indicated times using an epifluorescence microscope equipped with a video camera. The scale bar is 5 μ m.

in living cells has been demonstrated using Hoechst 33342 [26,27], each cell line must be analyzed individually to optimize the time of drug exposure and concentration of the drug [28]. Furthermore, as Hoechst 33342 is excited maximally near 350 nm and high intensities of ultraviolet (UV) irradiation can damage cells and produce cell cycle delay or arrest, the level of UV excitation must be controlled carefully. In addition, Hoechst 33342 affects cell cycle progression, arresting cells in G2 phase [29]. Intercalating DNA drugs, like dihydroethidium, may cause mutations in the DNA by interfering with DNA replication [28]. Microinjection of rhodamine-labeled histones, successfully used in *Drosophila* [8,9], is not suitable for analyzing a large population of mammalian cells. In contrast to these methods, the enhanced GFP [18] used in this study is excited with blue light (490 nm), which is less damaging than the UV-light excitation required for Hoechst. Moreover, constitutive expression of H2B-GFP from the integrated transgene enables long-term analyses without perturbing cell cycle progression (Figure 4). As the primary structures of histone proteins are well conserved among different species [30], it is likely that the H2B-GFP described here will be useful for cells of different species. This notion is supported by our ability to use the H2B-GFP vector in mouse, hamster, and monkey cells (data not shown).

The H2B-GFP strategy described in this report has a wide variety of applications for studying chromosome dynamics. For example, it can be used as a transfection marker that readily enables one to identify mitotic cells using fluorescence microscopy. H2B-GFP fluorescence persists in cells fixed in ethanol (Figure 4), which is useful for FACS analyses. As the intensity of H2B-GFP fluorescence depends on the chromosome condensation states in interphase cells (Figure 6), one can study chromosome condensation and decondensation in live cells [9]. The method may be especially useful for real-time analysis of apoptosis by enabling visualization of chromatin fragmentation and hypercondensation in living cells, as well as for studies of the effects of oncogenes on chromosome stability during tumor progression [31].

Using a retroviral vector expressing H2B-GFP, we have demonstrated that both normal chromosomes and small DMs can be readily distinguished in live cells. H2B-GFP enabled the observation of chromosomes in their native state without the need for fixation and permeabilization procedures, which can cause artificial distortion of intracellular structures. Our observations validate and extend a previous report in which DMs in fixed mitotic cells were observed to associate with the condensed chromosomes [5,6]. This led to a model for DM segregation involving 'hitch-hiking' of DMs on chromosomes [6]. The distinctive clustering behavior of DMs and their close association with normal chromosomes (Figures 7,8) provide one mechanism by which DMs are transmitted to daughter cells even though they lack functional centromeres. Clustered DMs appear to transmit to daughter cells in a highly stochastic manner, however. As COLO320DM cells grow faster when their levels of *c-myc* expression are elevated [4], daughter cells containing more DMs should be selected, and over time the population of cells will come to contain many DMs per cell. Therefore, although the number of DMs per cell is continuously changing by stochastic uneven distribution to daughter cells, DMs appear to be stably maintained when one considers the entire population. Sometimes, clustered DMs associate with both groups of the segregating daughter chromosomes, forming bridges across the midplane of anaphase cells (Figure 7b). It is tempting to speculate that such chromosomal bridges could increase chromosomal instability by inducing non-disjunction or, in some cases, by preventing chromosome segregation and increasing the probability of a chromosome arm being severed during cytokinesis. Were breakage to occur within an arm, genomic instability could be further increased by inheritance of the broken chromosome, which could initiate a bridge-breakage fusion cycle [32].

The mechanism of DM clustering during mitosis remains to be elucidated. One possibility is that DMs cluster due to their interaction with the spindle microtubules, as

interaction of non-centromeric chromatin with the mitotic spindle is well documented [33]. Chromosome spreads of colcemid-treated cells reveal a scattered distribution of DMs (Figure 7c), suggesting that spindle microtubules may play an important role in DM clustering. Alternatively, DMs themselves may have cohesive properties and may 'stick' to each other. It has been reported that a hamster cell line containing large tandemly repeated amplicons including the dihydrofolate reductase gene also had anaphase-bridge formations due to delayed sister-chromatid disjunction [34]. Repeated arrays of amplicons in DMs may have configurations that favor DM clustering and delayed disjunction of sister minute chromosomes during anaphase. The interaction between DMs and normal chromosomes must be clarified as well. The H2B-GFP system described here should facilitate the additional analyses required to understand the precise mechanism of DM clustering and segregation.

Conclusions

We have established a novel system for labeling chromatin in living cells using a fusion protein of histone H2B and GFP. The H2B-GFP system allows chromosomes, including DMs, to be imaged at a high resolution without perturbing cell cycle control or intracellular structures. The application of this system has revealed the distinctive clustering behavior of DMs in living mitotic cells. We propose that DM clustering is an important factor leading to their asymmetric distribution to daughter cells.

Materials and methods

Construction of H2B-GFP expression vectors

A human *H2B* gene was obtained by PCR amplification of human placental genomic DNA using primers which introduce *KpnI* and *BamHI* sites at the ends of one of the reported *H2B* sequences (GenBank accession number X00088) [35]: primer 1, 5'-CGGGTACCGCCAC-CATGCCAGAGCCAGCGAAGTCTGCT-3'; primer 2, 5'-CGGGATC-CTTAGCGTGGTGTACTTGGTGAC-3'. Primer 1 introduced the Kozak consensus sequence in front of the initiation codon. PCR reaction parameters were as follows: 95°C for 10 min, 25 cycles at 94°C for 1 min, 50°C for 1 min, 72°C for 2 min, followed by 72°C for 5 min. One of the obtained clones, which was 98.4% identical to the *H2B* gene (X00088), was used to construct the H2B-GFP vector. The PCR product was digested with *KpnI* and *BamHI* and subcloned into the cloning site of pEGFPN1 vector (Clontech) [18]. The H2B-GFP chimeric gene was subcloned into a mammalian expression vector (J. Kolman, T.K., unpublished observations). H2B-GFP expression was driven by the EF-1 α promoter, a strong promoter in mammalian cells [36]. The vector contained the blasticidin resistance gene [37] as a selection marker. A retroviral vector, pCLNC-H2BG, was constructed by cloning the H2B-GFP gene into the pCLNCX vector [38]. Cloning details are available upon request.

Cell lines and transfection

HeLa cells were grown as monolayers in Dulbecco's modified Eagle's medium (DMEM) supplemented with 10% fetal calf serum (FCS). Exponentially growing cells (in 10 cm dishes) were transfected with 20 μ g H2B-GFP expression vector using a calcium phosphate precipitation protocol [39]. Transfected cells were replated 48 h after transfection and 5 μ g ml⁻¹ blasticidin-S (Calbiochem) was added 72 h after transfection. Five days later, the medium was changed to 2 μ g ml⁻¹ blasticidin-S. After 15 days of drug selection, surviving

colonies were checked under fluorescence microscopy and GFP-positive colonies were isolated. Several clones were selected and expanded into cell lines for further analyses. Production of VSV-G pseudotyped retrovirus [23] was performed by co-transfection of pCLNC-H2BG and pMD.G (the plasmid encoding the envelope protein VSV-G) into 293 gp/bsr cells as described [40]. COLO320DM cells [24] were grown in RPMI1640 medium supplemented with 10% FCS. Exponentially growing cells (in 10 cm dishes) were incubated with the concentrated viral supernatants in the presence of $8 \mu\text{g ml}^{-1}$ Polybrene (Aldrich). After overnight incubation, medium was changed and the infected cells were expanded for further analyses without drug selection.

Mononucleosome preparation

Mononucleosomes were purified according to the protocol (kindly provided by T. Ito and J. Kadonaga) [19] with several modifications. HeLa cells and stable cells expressing H2B-GFP (3×10^7) were trypsinized, harvested and washed once with $1 \times$ RSB buffer (10 mM Tris pH 7.6, 15 mM NaCl, 1.5 mM MgCl_2). After centrifugation, the cell pellet was resuspended in $1 \times$ RSB buffer with 1% Triton-X 100, homogenized by five strokes with a loose-fitting pestle to release nuclei. Nuclei were collected by centrifugation and washed twice with 1 ml buffer A (15 mM Tris pH 7.5, 15 mM NaCl, 60 mM KCl, 0.34 M sucrose, 0.5 mM spermidine, 0.15 mM spermine, 0.25 mM PMSF and 0.1% β -mercaptoethanol). Nuclei were finally resuspended in 1.5 ml buffer A and $15 \mu\text{l}$ 0.1 M CaCl_2 was added.

For making nucleosomal ladders, 0.5 ml suspended nuclei were digested by adding $1 \mu\text{l}$ micrococcal nuclease (Sigma, 200 units ml^{-1}) at 37°C . Aliquots (60 μl) were taken at each time point (1, 5, 10, 15, 30, 60 min) and $1.5 \mu\text{l}$ of 0.5 M EDTA was added to stop the reaction. To each tube, 18 μl H_2O , 12 μl 10% SDS and 24 μl 5 M NaCl were added. The mixtures were extracted with phenol-chloroform and 5 μl supernatant was analyzed by 1.5% agarose gel electrophoresis.

Limit digests for making mononucleosomes were performed by adding $10 \mu\text{l}$ micrococcal nuclease (200 units ml^{-1}) to 1.0 ml suspended nuclei. After 2 h digestion at 37°C , $20 \mu\text{l}$ 0.5 M EDTA was added to stop the reaction. The digest was centrifuged at 10,000 rpm for 10 min and the supernatant was collected. The pellet (chromatin fraction) was resuspended in 450 μl 10 mM EDTA, 50 μl 5 M NaCl was added to solubilize it, and the mixture was centrifuged at 14,000 rpm for 5 min to remove debris. The chromatin fraction was further fractionated on a 5–30% sucrose gradient for 18 h at 26,000 rpm in a Beckman SW41 rotor. After centrifugation, 1 ml fractions were collected and small aliquots (50 μl) of each sample were taken for DNA analyses. The remainder of each sample (950 μl) was precipitated with 280 μl 100% TCA with deoxycholic acid and left on ice for 10 min. The samples were then centrifuged at 3000 rpm for 5 min and each pellet was washed with acetone followed by a 70% ethanol wash. The pellet was air dried and resuspended in 20 μl of $1 \times$ SDS sample buffer, and aliquots were analyzed by gel electrophoresis through SDS–15% polyacrylamide gels followed by Coomassie staining. Western blotting was performed using anti-human-H2B antibody (1:1000, Chemicon) as a primary antibody. Signals were detected by enhanced luminol reagents (NEN Life Science Products) according to the manufacturer's instructions.

FACS analyses

HeLa cells and HeLa cells expressing H2B-GFP were harvested by trypsinization, fixed in 70% ethanol for 3 h at 4°C . Cells were stained with PI ($20 \mu\text{g ml}^{-1}$) containing RNase (200 ng ml^{-1}). Fluorescence was measured using a FACScan (Becton Dickinson). The red (PI) and green (GFP) emissions from each cell were separated and measured using standard optics. Color compensation was done to eliminate the artifact due to the overlap of PI and GFP emission. Cell debris and fixation artifacts were gated out. Data analysis was done using Cell Quest software (Becton Dickinson), and G1, S, and G2/M fractions were quantified using Multicycle software (Phoenix flow systems).

Fluorescence microscopy

For chromosome spreads, HeLa cells expressing H2B-GFP were treated with colcemid (100 ng ml^{-1}) for 1 h, trypsinized, harvested, and resuspended in hypotonic buffer (10 mM Tris pH 7.4, 10 mM NaCl, 5 mM MgCl_2 ; 1.5×10^6 cells ml^{-1}) for 10 min. Swollen cells (50 μl) were attached to poly-L-lysine coated slide glasses by cytospin (90 sec), fixed in 3.7% formaldehyde for 5 min, 0.1% NP40 in phosphate-buffered saline for 10 min and counterstained with DAPI ($1 \mu\text{g ml}^{-1}$). Images were collected with a Nikon fluorescence microscope equipped with either DAPI or fluorescein isothiocyanate (FITC) filter sets.

Immunofluorescence with a human anti-centromere antiserum was performed as described previously [41]. Microscopy was performed on a BioRad 1024 confocal microscope built on a Zeiss Axiovert 100 using a $63 \times 1.4 \text{ NA}$ Zeiss Plan Achromat objective lens.

FISH was performed as previously described using a biotinylated *c-myc* cosmid probe and FITC-avidin [25]. For *in situ* fixation, asynchronously growing COLO320DM cells were directly fixed on chamber slides (Lab-Tek) without colcemid treatment as described [31].

To visualize H2B-GFP in living cells, cells were grown on 25 mm coverslips and mounted with prewarmed culture medium in a Dvorak-Stotler chamber (Lucas-Highland Company). Images were collected on the BioRad 1024 confocal microscope described above using either the $63 \times$ lens or a $40 \times 1.3 \text{ NA}$ Neofluar objective using a laser power of 0.3–1% for GFP fluorescence. Transmitted light images were collected with DIC optics. Fluorescence images were overlaid onto DIC images using Adobe Photoshop. Z-series images were collected and stereoscopic images were made using the BioRad software supplied with the microscope.

For time-lapse microscopy, cells were cultured in 35 mm glass-bottom culture dishes (Mat Tek Corporation). The culture medium was supplemented with 20 mM HEPES pH 7.3 and mineral oil was overlaid to cover the surface of the medium. The dishes were mounted on a Nikon inverted fluorescence microscope (Diaphot 300) equipped with a video camera (CCD72; MTI). The temperature of the medium was kept constant at 37°C using a heated stage. A $100 \times 1.3 \text{ NA}$ oil-immersion lens was used for observation. Images were acquired using IP Lab spectrum software (Signal Analytics Corporation).

Acknowledgements

We thank J. Kolman for providing the backbone vector for H2B-GFP expression, F. Hanaoka for the blasticidin resistance gene, T. Ito and J. Kadonaga for the mononucleosome purification protocol, N. Somia and I. Verma for 293 gp/bsr cells, M. Friedlander and T. Hope for generously allowing us to use their microscopy systems, Wahl lab members for critically reading the manuscript and for their encouragement, R. Rubin for his helpful comments about nucleosomes, D. Chambers for the FACS analysis and M. Urista for her technical assistance. This work was supported by a grant from the Department of the Army, Grant number DAMD17-94-J4359 and by the G. Harold and Leila Y. Mathers Charitable Foundation (G.M.W.), and a grant from the National Institute for General Medical Sciences, GM39068 (K.F.S.).

References

- Benner SE, Wahl GM, Von Hoff DD: Double minute chromosomes and homogeneously staining regions in tumors taken directly from patients versus in human tumor cell lines. *Anticancer Drugs* 1991, 2:11–25.
- Cowell JK: Double minutes and homogeneously staining regions: gene amplification in mammalian cells. *Annu Rev Genet* 1982, 16:21–59.
- Stark GR, Wahl GM: Gene amplification. *Annu Rev Biochem* 1984, 53:447–491.
- Von Hoff DD, McGill JR, Forseth BJ, Davidson KK, Bradley TP, Van DD, et al.: Elimination of extrachromosomally amplified MYC genes from human tumor cells reduces their tumorigenicity. *Proc Natl Acad Sci USA* 1992, 89:8165–8169.

5. Barker PE, Hsu TC: Are double minutes chromosomes? *Exp Cell Res* 1978, **113**:456-458.
6. Levan A, Levan G: Have double minutes functioning centromeres? *Hereditas* 1978, **88**:81-92.
7. Wolffe A: *Chromatin: Structure and Function*, 2nd edn. San Diego: Academic Press; 1995.
8. Minden JS, Agard DA, Sedat JW, Alberts BM: Direct cell lineage analysis in *Drosophila melanogaster* by time-lapse, three-dimensional optical microscopy of living embryos. *J Cell Biol* 1989, **109**:505-516.
9. Hiraoka Y, Minden JS, Swedlow JR, Sedat JW, Agard DA: Focal points for chromosome condensation and decondensation revealed by three-dimensional *in vivo* time-lapse microscopy. *Nature* 1989, **342**:293-296.
10. Chalfie M, Tu Y, Euskirchen G, Ward WW, Prasher DC: Green fluorescent protein as a marker for gene expression. *Science* 1994, **263**:802-805.
11. Cubitt AB, Heim R, Adams SR, Boyd AE, Gross LA, Tsien RY: Understanding, improving and using green fluorescent proteins. *Trends Biochem Sci* 1995, **20**:448-455.
12. Gerdes HH, Kaether C: Green fluorescent protein: applications in cell biology. *FEBS Lett* 1996, **389**:44-47.
13. Misteli T, Spector DL: Applications of the green fluorescent protein in cell biology and biotechnology. *Nat Biotechnol* 1997, **15**:961-964.
14. Robinett CC, Straight A, Li G, Wilhelm C, Sudlow G, Murray A, *et al.*: *In vivo* localization of DNA sequences and visualization of large-scale chromatin organization using lac operator/repressor recognition. *J Cell Biol* 1996, **135**:1685-1700.
15. Straight AF, Belmont AS, Robinett CC, Murray AW: GFP tagging of budding yeast chromosomes reveals that protein-protein interactions can mediate sister chromatid cohesion. *Curr Biol* 1996, **6**:1599-1608.
16. Shelby RD, Hahn KM, Sullivan KF: Dynamic elastic behavior of alpha-satellite DNA domains visualized *in situ* in living human cells. *J Cell Biol* 1996, **135**:545-557.
17. Flach J, Bossie M, Vogel J, Corbett A, Jinks T, Willins DA, *et al.*: A yeast RNA-binding protein shuttles between the nucleus and the cytoplasm. *Mol Cell Biol* 1994, **14**:8399-8407.
18. Yang TT, Cheng L, Kain SR: Optimized codon usage and chromophore mutations provide enhanced sensitivity with the green fluorescent protein. *Nucleic Acids Res* 1996, **24**:4592-4593.
19. Laybourn PJ, Kadonaga JT: Role of nucleosomal cores and histone H1 in regulation of transcription by RNA polymerase II. *Science* 1991, **254**:238-245.
20. Belmont AS, Bruce K: Visualization of G1 chromosomes: a folded, twisted, supercoiled chromonema model of interphase chromatid structure. *J Cell Biol* 1994, **127**:287-302.
21. Moroi Y, Hartman AL, Nakane PK, Tan EM: Distribution of kinetochore (centromere) antigen in mammalian cell nuclei. *J Cell Biol* 1981, **90**:254-259.
22. Bartholdi MF: Nuclear distribution of centromeres during the cell cycle of human diploid fibroblasts. *J Cell Sci* 1991, **99**:255-263.
23. Burns JC, Friedmann T, Driever W, Burrascano M, Yee JK: Vesicular stomatitis virus G glycoprotein pseudotyped retroviral vectors: concentration to very high titer and efficient gene transfer into mammalian and nonmammalian cells. *Proc Natl Acad Sci USA* 1993, **90**:8033-8037.
24. Alitalo K, Schwab M, Lin CC, Varmus HE, Bishop JM: Homogeneously staining chromosomal regions contain amplified copies of an abundantly expressed cellular oncogene (c-myc) in malignant neuroendocrine cells from a human colon carcinoma. *Proc Natl Acad Sci USA* 1983, **80**:1707-1711.
25. Shimizu N, Kanda T, Wahl GM: Selective capture of acentric fragments by micronuclei provides a rapid method for purifying extrachromosomally amplified DNA. *Nat Genet* 1996, **12**:65-71.
26. Belmont AS, Braunfeld MB, Sedat JW, Agard DA: Large-scale chromatin structural domains within mitotic and interphase chromosomes *in vivo* and *in vitro*. *Chromosoma* 1989, **98**:129-143.
27. Hiraoka Y, Haraguchi T: Fluorescence imaging of mammalian living cells. *Chromosome Res* 1996, **4**:173-176.
28. Arndt-Jovin DJ, Jovin TM: Fluorescent labeling and microscopy of DNA. *Methods Cell Biol* 1989, **30**:417-448.
29. Tobey RA, Oishi N, Crissman HA: Cell cycle synchronization: reversible induction of G2 synchrony in cultured rodent and human diploid fibroblasts. *Proc Natl Acad Sci USA* 1990, **87**:5104-5108.
30. Wells DE: Compilation analysis of histones and histone genes. *Nucleic Acids Res* 1986, **14**:R119-R149.
31. Denko N, Stringer J, Wani M, Stambrook P: Mitotic and post-mitotic consequences of genomic instability induced by oncogenic Ha-ras. *Somat Cell Mol Genet* 1995, **21**:241-253.
32. Coquelle A, Pipiras E, Toledo F, Buttin G, Debatisse M: Expression of fragile sites triggers intrachromosomal mammalian gene amplification and sets boundaries to early amplicons. *Cell* 1997, **89**:215-225.
33. Fuller MT: Riding the polar winds: chromosomes motor down east. *Cell* 1995, **81**:5-8.
34. Warburton PE, Cooke HJ: Hamster chromosomes containing amplified human alpha-satellite DNA show delayed sister chromatid separation in the absence of *de novo* kinetochore formation. *Chromosoma* 1997, **106**:149-159.
35. Zhong R, Roeder RG, Heintz N: The primary structure and expression of four cloned human histone genes. *Nucleic Acids Res* 1983, **11**:7409-7425.
36. Mizushima S, Nagata S: pEF-BOS, a powerful mammalian expression vector. *Nucleic Acids Res* 1990, **18**:5322.
37. Izumi M, Miyazawa H, Kamakura T, Yamaguchi I, Endo T, Hanaoka F: Blasticidin S-resistance gene (bsr): a novel selectable marker for mammalian cells. *Exp Cell Res* 1991, **197**:229-233.
38. Naviaux RK, Costanzi E, Haas M, Verma IM: The pCL vector system: rapid production of helper-free, high-titer, recombinant retroviruses. *J Virol* 1996, **70**:5701-5705.
39. Chen C, Okayama H: High-efficiency transformation of mammalian cells by plasmid DNA. *Mol Cell Biol* 1987, **7**:2745-2752.
40. Miyoshi H, Takahashi M, Gage FH, Verma IM: Stable and efficient gene transfer into the retina using an HIV-based lentiviral vector. *Proc Natl Acad Sci USA* 1997, **94**:10319-10323.
41. Sullivan KF, Hechenberger M, Masri K: Human CENP-A contains a histone H3 related histone fold domain that is required for targeting to the centromere. *J Cell Biol* 1994, **127**:581-592.

Because *Current Biology* operates a 'Continuous Publication System' for Research Papers, this paper has been published on the internet before being printed. The paper can be accessed from <http://biomednet.com/cbiology/cub> - for further information, see the explanation on the contents page.